Scintilla: Simulating Combustible Vegetation for Wildfires

ANDRZEJ KOKOSZA, AMU, Poland
HELGE WREDE, CAU, Germany
DANIEL GONZALEZ ESPARZA, KAUST, KSA
MILOSZ MAKOWSKI, AMU, Poland
DAOMING LIU, KAUST, KSA
DOMINIK L. MICHELS, KAUST, KSA
SÖREN PIRK, CAU, Germany
WOJTEK PAŁUBICKI, AMU, Poland

Fig. 1. A temporal progression of a wildfire generated with our framework. Modeling different types of fuel and vegetation with detailed geometry enables simulating complex wildfire behavior ranging from harmless surface fires to raging crown fires.

Authors' addresses: Andrzej Kokosza, andkok@amu.edu.pl, AMU, Uniwersytetu Poznańskiego 4, 61-614, Poznań, Poland; Helge Wrede, hew@informatik.uni-kiel.de, CAU, Christian-Albrechts-Platz 4, 24118 Kiel, Germany; Daniel Gonzalez Esparza, daniel.gonzalezesparza@kaust.edu.sa, KAUST, Visual Computing Center, Thuwal 23955, KSA; Milosz Makowski, milosz.makowski@amu.edu.pl, AMU, Uniwersytetu Poznańskiego 4, 61-614, Poznań, Poland; Daoming Liu, liudaoming3@gmail.com, KAUST, Visual Computing Center, Thuwal 23955, KSA; Dominik L. Michels, dominik.michels@kaust.edu.sa, KAUST, Visual Computing Center, Thuwal 23955, KSA; Sören Pirk, soeren.pirk@gmail.com, CAU, Christian-Albrechts-Platz 4, 24118 Kiel, Germany; Wojtek Pałubicki, wojciech.palubicki@amu.edu.pl, AMU, Uniwersytetu Poznańskiego 4, 61-614, Poznań, Poland.

0730-0301/2023/12-ART000
https://doi.org/00.0000/0000000.0000000

Wildfires are a complex physical phenomenon that involves the combustion of a variety of flammable materials ranging from fallen leaves and dried twigs to decomposing organic material and living flora. All these materials can potentially act as fuel with different properties that determine the progress and severity of a wildfire. In this paper, we propose a novel approach for simulating the dynamic interaction between the varying components of a wildfire, including processes of convection, combustion and heat transfer between vegetation, soil and atmosphere. We propose a novel representation of vegetation that includes detailed branch geometry, fuel moisture, and distribution of grass, fine fuel, and duff. Furthermore, we model the ignition, generation, and transport of fire by firebrands and embers. This allows simulating and rendering virtual 3D wildfires that realistically capture key aspects of the process, such as progressions from ground to crown fires, the impact of embers carried by wind, and the effects of fire barriers and other human intervention methods. We evaluate our approach through numerous experiments and based on comparisons to real-world wildfire data.

CCS Concepts: • **Computing methodologies** → **Physical simulation**.

Additional Key Words and Phrases: Branch Litter, Combustion, Fire Spotting, Fire Spread, Fluid Dynamics, Grass, Level of Detail, Numerical Simulation, Physics-based Modeling, Understory, Vegetation, Wildfires.

ACM Reference Format:
Andrzej Kokosza, Helge Wrede, Daniel Gonzalez Esparza, Milosz Makowski, Daoming Liu, Dominik L. Michels, Sören Pirk, and Wojtek Pałubicki. 2023. Scintilla: Simulating Combustible Vegetation for Wildfires. *ACM Trans. Graph.* 00, 0, Article 000 (December 2023), 20 pages. https://doi.org/00.0000/0000000.0000000

1 INTRODUCTION

Wildfires are disastrous natural phenomena that ravage communities and ecosystems alike. The Black Summer bushfire in Australia was a particularly severe example where an extensive area was burnt with more than one billion animal deaths [Abram et al. 2021]. A wildfire is the uncontrolled and often unpredictable combustion of vegetation that not only includes trees and shrubs, but also other types of fuel, such as grass, duff, dead leaves and needles. These destructive events rapidly consume vast areas, leading to loss of life, property, and severe ecological damage. However, the underlying mechanisms that lead from a smouldering ground combustion to a blazing crown fire are complex processes that are not fully understood. Therefore, to advance our understanding of the dynamics and progression of wildfires, we argue that it is critical to carefully simulate the feedback loops of vegetation, the atmosphere, and the composition of different fuels. By creating realistic 3D simulations, it is not only possible to enable applications such as training firefighters for wildfire management but also complex CG effects for movies or games.

A number of approaches have recently addressed generating more realistic models of ecosystems and the related physical processes between vegetation and the atmosphere. These methods range from efficient representations for large-scale ecosystems [Kapp et al. 2020; Makowski et al. 2019] and urban forests [Niese et al. 2022] to the response of vegetation to erosion [Cordonnier et al. 2017], avalanches [Cordonnier et al. 2018], and climatic gradients [Pałubicki et al. 2022]. In computer graphics, only a few methods address simulating the combustion of trees [Pirk et al. 2017] and wildfires [Hädrich et al. 2021] with detailed geometry. Coupling intricate plant geometry with complex fluid dynamics, while also simulating the combustion process of fuel, remains a challenging objective. To the best of our knowledge, no method has simulated the various types of fuels that are represented by the understory and forest floor of an ecosystem.

In this paper, we propose a unified multi-scale representation for simulating wildfires. We generate 3D models of trees and shrubs based on branch modules – each plant is defined as a collection of modules that locally adapt to their environment. Based on this formulation we can efficiently model large-scale forest ecosystems. Plant matter that commonly defines the understory and forest floor, such as smaller plants, duff, and fine fuel, is represented by a novel layer-based representation that is integrated with the wildfire simulation. To simulate the horizontal as well as the vertical fire spread, we define a novel mathematical framework for heat transfer between the different fuel domains.

Unlike existing approaches in computer graphics, our unified framework can simulate all commonly described types of wildfires, including ground fires, surface fires, and crown fires in various stages. Furthermore, our approach realistically captures wildfires in different biomes, ranging from grassland, shrubland, savannah, tundra to boreal and deciduous forests. By including a detailed representation of vegetation our method captures the plausible dynamics of wildfires and its behavior when subjected to various human forest management protocols. Furthermore, we include comparisons to controlled burn experiments that demonstrate that the emergent phenomena expressed with our simulations correspond to those observed in reality. Finally, to account for fire spotting due to sparks and flying embers, we advect particles through the air to then ignite fuel once they again make contact with vegetation to better express the unpredictable nature of wildfires.

In Fig. 1 we show a rendering of a complex wildfire created with our framework; animations of the simulation can be found in the accompanying video. The simulation parameter values have been set to define an active crown fire which is combusting most of the vegetation that has been distributed in the scene. In summary, the contributions of our paper are: We introduce (1) a novel fuel moisture model that accounts for a realistic distribution of fuel moisture in a forest biome as well as its integration into the wildfire simulation; (2) a boundary fuel model describing the impact of grass, fine fuel, and duff layers in a wildfire; (3) a physically-plausible model that captures the realistic generation, transportation and ignition of embers and firebrands that can produce new fires ahead of the fire front.

2 RELATED WORK

Modeling wildfires is a strictly interdisciplinary topic that spans a range of fields and methods that we cannot conclusively discuss. Therefore, we aim to provide an overview of modeling vegetation and outdoor environments, simulating fire, and methods that specifically focus on wood combustion and wildfires.

Modeling Vegetation. Due to the complexity of vegetation early methods for generating branching structures have focused on exploiting the self-similar nature of trees with fractals [Aono and Kunii 1984], repetitive patterns [Oppenheimer 1986], L-Systems [Prusinkiewicz 1986], or rule-based approaches [Lintermann and Deussen 1999], a review is provided in Palubicki et al. [2019]. In the more recent past, these methods have been extended to procedural modeling algorithms that often also consider biological findings to express phenomenological or self-organizing growth of trees [Guo et al. 2020; Palubicki et al. 2009; Runions et al. 2007; Stava et al. 2014]. It has been recognized that models of trees and plants can be reconstructed from point clouds [Livny et al. 2011; Xu et al. 2007] or images [Bradley et al. 2013; Neubert et al. 2007; Quan et al. 2006; Tan et al. 2008]; efforts that have recently been facilitated due to the availability of neural networks that are able to first encode the captured sensor data to intermediate representations [Kałużny et al. 2024; Li et al. 2021; Liu et al. 2021; Zhou et al. 2023]. Sketch-based methods, on the other hand, enable users to design plant models

so as to satisfy artistic requirements [Ijiri et al. 2006; Okabe et al. 2007], also in combination with procedural algorithms [Longay et al. 2012], or guided by envelope shapes [Benes et al. 2009; Wither et al. 2009]. Besides the modeling of branching structures, a few methods focus on simulating the dynamics of vegetation. Approaches exists to capture how plants develop in different environmental conditions [Maggioli et al. 2023; Měch and Prusinkiewicz 1996; Pirk et al. 2012b; Wong and Chen 2015], to animate the growth of plants [Hädrich et al. 2017; Pirk et al. 2012a] and their response to wind [Habel et al. 2009; Pirk et al. 2014; Quigley et al. 2018; Shao et al. 2021], and the interaction of root systems in different soil types [Li et al. 2023].

Modeling Outdoor Environments. A range of methods targets the modeling of large-scale terrains by generating distributions of plant populations [Deussen et al. 1998; Lane and Prusinkiewicz 2002] or by defining their placement with procedural algorithms [Niese et al. 2022]. To manage the complexity of large-scale ecosystems a number of methods focus on defining geometric representations for vegetation. This ranges from layers [Argudo et al. 2017], billboard clouds [Behrendt et al. 2005], and voxels [Jaeger and Teng 2003] to volumetric textures [Bruneton and Neyret 2012] and stochastic pruning [Neubert et al. 2011]. The approach of Makowski et al. [2019] simulates ecosystems by growing individual trees based on modules that represent individual branches. Modeling trees based on modules has shown to be a versatile representation to facilitates modeling large-scale ecosystems according to changing climatic gradients [Pałubicki et al. 2022] and in response to wildfires [Hädrich et al. 2021]. On a different trajectory a number of methods have been developed to author forest ecosystems according to user-feedback [Benes et al. 2009; Cordonnier et al. 2017] that can even be combined with the predictive capabilities of neural networks [Kapp et al. 2020]. Besides modeling forests, several approaches focus on modeling other types of ecosystems and outdoor landmarks, such as deserts [Paris et al. 2019], rivers [Peytavie et al. 2019], glaciers [Argudo et al. 2020], and even agricultural fields [Cieslak et al. 2024]. Moreover, a number of recent methods started to more carefully combine terrain and atmosphere modeling to generate realistic cloud species [Hädrich et al. 2020; Vimont et al. 2020], and different types of weather [Herrera et al. 2021].

Simulating Fire and Combustion. Simulating fire and smoke with computational fluid dynamics has received a considerable amount of research attention in the past [Bridson and Müller 2007; Huang et al. 2014]. To capture high-frequency details of the fluid dynamics, a majority of methods leverages grid-based fluid solvers for smoke [Fedkiw et al. 2001; Pan and Manocha 2017; Rasmussen et al. 2003] and fire [Hong et al. 2010; Nguyen et al. 2002; Stam 1999]. Several methods focus on the visual modeling of fire, either based on physically-based models [Nguyen et al. 2002; Pegoraro and Parker 2006], with a focus on flame properties [Nguyen et al. 2001], by enabling artistic control [Lamorlette and Foster 2002], or based on particle representations [Horvath and Geiger 2009]. For combustion, existing methods have focused on the distribution of heat [Melek and Keyser 2002] on surfaces [Chiba et al. 1994], within volumes [Zhao et al. 2003], or based on disconnected propagating fronts [Liu et al. 2012]. More recent physics-based approaches focus on carefully modeling the thermodynamic properties of real fuels

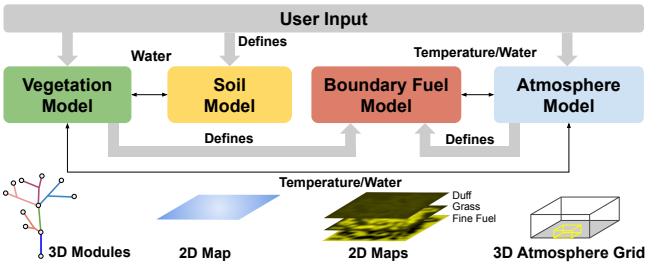

Fig. 2. An overview of our method. A user specifies the initialization of vegetation, soil and atmosphere models as inputs. We then initialize the boundary fuel model. Wildfires are simulated by representing the fuel, water and other wildfire related quantities using a multi-domain approach, which includes 3D modules for representing plants, 2D maps for representing the soil and the forest floor, and a 3D grid for representing the atmosphere.

to simulate deflagration phenomena, such as different flame types, fireballs, and even subsonic explosions [Nielsen et al. 2022], or the melting and solidification of material [Stomakhin et al. 2014].

Wood Combustion and Wildfires. A wide range of modeling approaches aims at expressing the complexity of wildfire behavior and the combustion of wood. This spans from approaches for defining the pyrolysis process [Bohren and Thorud 1973] and charring [Lizhong et al. 2002] to simulating the heat transfer [Encinas et al. 2007]. Several studies investigate the resistance of plant species to wildfires [Lawes et al. 2011; Zylstra 2021] and the impact of the moisture content of fuel [Masinda et al. 2020]. It also has been recognized that the architecture of the canopy plays a role in the spread of wildfires [Schwilk 2003]. Many existing methods focus on identifying parsimonious mathematical formalisms to analyze and predict wildfire behavior [Coen 2013; Katan and Perez 2021; Mandel et al. 2014; Monedero et al. 2017; Pastor et al. 2003; Richards 1990; Vanella et al. 2021]. This includes models for the ignition of wildfires [Anand et al. 2017], the interaction of wildfires with the atmosphere [Masinda et al. 2020] or simple geometric shapes as proxies objects for vegetation [Mendoza et al. 2019]. Moreover, the behavior of wildfires is also studied specifically for different types of biomes [Cheney et al. 1993; Dupuy and Larini 2000]. Existing simulation methods include empirical, physical, and even hybrid models, often relying on computational fluid dynamics [McGrattan et al. 2012] and large eddy simulations [Filippi et al. 2018]. Finally, a number of methods investigates the fire spread according to different fuel types [Aragoneses and Chuvieco 2021; Mell et al. 2007]. For an overview on combustion processes the reader is referred to [McAllister et al. 2011]. Unlike these methods, we propose a novel mathematical framework based on a unified formulation for detailed 3D plant models and other fuel types.

3 OVERVIEW

Our main goal is to extend the wildfire model of Hädrich et al. [2021], which relies on a grid-based fluid simulation coupled with a detailed vegetation representation. In contrast to them, our model emphasizes the role and coordinated action of different combustible materials such as grass, fine fuel, duff, and other vegetation, as well as the impact of fuel moisture, fire brands, and turbulence of fire. As input,

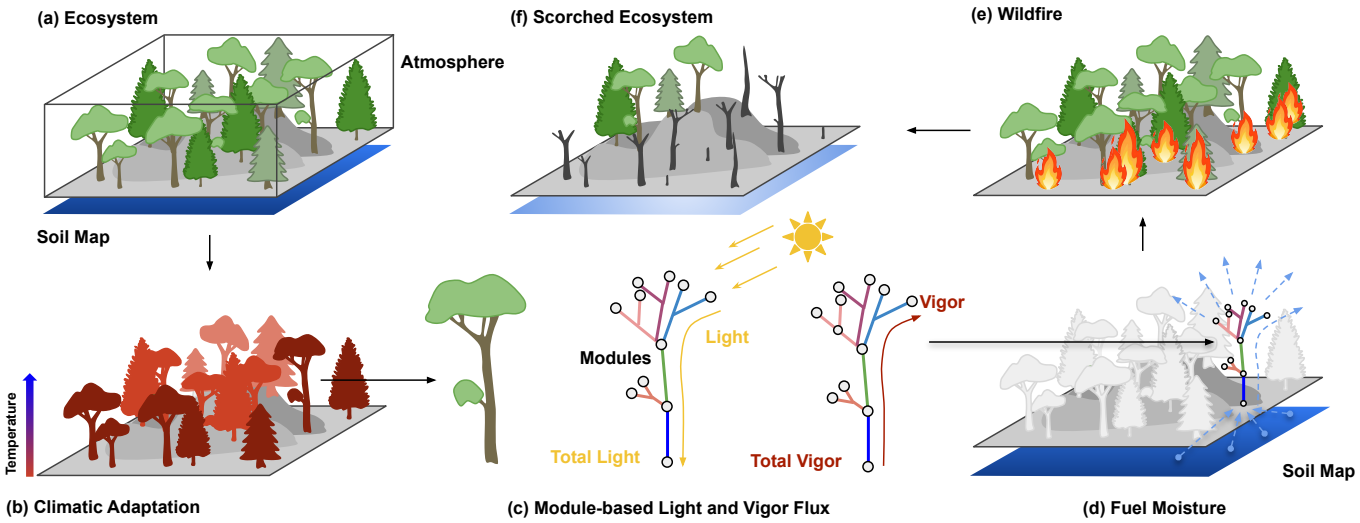

Fig. 3. Stages of our wildfire simulation method: the initial ecosystem consists of terrain and vegetation, an atmosphere model, and a soil map (a), serving as the simulation input. We calculate climatic adaptation parameters for all plants (b) – lighter red color intensity indicates less adapted plants to the cooler climate at higher altitude. In (c) we show the computation of light and vigor flux for each module of a plant that we use to compute fuel moisture (d). Finally, we can simulate a wildfire (e) which then leads to a scorched ecosystem (f).

our method uses a digital elevation model of the terrain with a soil water map, a set of multi-scale plant graphs [Godin and Caraglio 1998] representing branches, modules and plants, an atmosphere data structure for storing variations in pressure, humidity, temperature, and wind velocities, as well as a soil map representing the distribution of soil water in the scene. Before running the wildfire simulation we first compute the fuel moisture content of the vegetation at module-scale based on the input – plants can have a varying distribution of fuel moisture within their structure. Additionally, we calculate the distribution of other wildfire fuels based on the vegetation data and described by 2D spatial maps representing grass, fine fuel, and duff (the boundary fuel layer).

For simulating wildfire dynamics, we introduce a multi-domain approach that describes combustion and heat transfer for all these materials. Specifically, we simulate the transfer of heat between the 2D spatial maps, the 3D domain of the atmosphere, and the plant graphs. Once the vegetation, the boundary fuels, and the atmosphere are defined, a user may interactively initiate fires anywhere in the scene by locally raising the temperature to a sufficiently high degree. Our wildfire simulation then resolves a set of coupled partial differential equations defined over the various spatial domains to simulate the combustion of vegetation, the boundary fuel layer, as well as the generation and transport of firebrands. This allows our approach to plausibly simulate wildfires occurring in the ground, on the surface and through the canopy, enabling the realistic combustion of vegetation in different forest biomes. An overview of our method is shown in Fig. 2.

4 WILDFIRES

Wildfires in forest biomes can be highly unpredictable and dangerous, and their progression depends on a number of physical factors. Wildfires are typically initiated by a heat source such as lightning, human activity, or other natural events. Once a fire is ignited, it heats up the air and causes it to rise, which – in turn – draws in more oxygen and fuels to the fire. This process is known as convection, and it can cause the fire to grow rapidly. The flames can then leap from shrub to shrub, and embers can be carried by the wind to start new fires in other areas. Another physical phenomenon that can contribute to the spread of wildfires is radiant heat. As the flames burn, they emit heat that can ignite nearby vegetation even if the flames themselves do not reach it. This can cause the fire to spread more rapidly and unpredictably, making it difficult to contain. The rate at which a wildfire spreads also depends on the topography, the climate, and the type of biome, such as grassland, shrubland, forest or tundra.

Grassland wildfires tend to spread quickly and have a low to moderate intensity. The fine, continuous fuel bed of grasses allows for fast fire spread, while the relatively low biomass of the vegetation limits fire intensity. Grassland fires are often influenced by wind, and may spread more quickly in areas with steep slopes or narrow canyons. *Shrubland wildfires* can be highly unpredictable, with rapid fire spread and high intensity. The presence of woody shrubs and other vegetation creates a complex fuel structure that can burn with high heat and create significant smoke. *Forest wildfires* can be extremely intense and destructive, particularly when they burn in the upper canopy. The presence of large trees and the abundance of ladder fuels, such as small trees and shrubs, can allow fires to spread rapidly and reach great heights. Forest fires can also create their own weather, with powerful up- and downdrafts that can contribute to erratic fire behavior. Finally, *Tundra wildfires* typically burn in the upper soil layer, as the vegetation is low-growing and sparse. The low biomass of the vegetation limits fire intensity, but the flammable peat soils common in some tundra ecosystems can allow fires to smolder underground and persist for weeks or even months.

5 MODEL

We introduce a wildfire model that describes the coordinated combustion of various organic fuels, such as wood, grass, and decomposing organic matter that enables the simulation of plausible wildfire dynamics in different forest biomes.

5.1 Hypotheses

Our wildfire model is a fluid dynamical system coupled with multiple subcomponents which formalizes the description provided in Sec 3. Specifically, we aim to describe a set of hypotheses capturing the essential processes controlling the dynamics of wildfires:

(1) Organic material under heat is decomposed into char, vapor, and flammable gases (combustion); Eqs. 2, 13.
(2) The rate at which organic material is combusted depends on it's type, temperature and moisture content (fuel moisture); Eq. 14.
(3) Thicker organic tissue that produces char undergoes pyrolysis and the region where this process occurs is approximated by a surface (pyrolyzing front); Eq. 13.
(4) Temperature in the atmosphere and vapor are advected by the wind field (convection); see Sec. 4.3 [Hädrich et al. 2021].
(5) Burning organic material may transfer heat to other organic materials and the atmosphere (radiant heat); see Sec. 5.6.
(6) Grass amount per unit area is proportional to light availability, temperature, and soil water; Eq. 6.
(7) Fine fuel amount per unit area is proportional to plant biomass and type; Eq. 7.
(8) Duff amount per unit area is proportional to plant biomass, type, and soil water; Eq. 8.

Hypotheses (1)-(3) describe the combustion of organic material (pyrolysis). They are defined for the multi-scale plant graph representation of our wildfire model. Hypotheses (4) and (5) describe the coordinated action of wildfire components which are shared among other simulated spaces such as fuel, heat, water, and vapor transfer. Finally, hypotheses (6)-(8) describe how grass, fine fuel, and duff amounts are defined for a given a scene.

5.2 Spaces

Our wildfire model comprises several spatial domains, each representing a distinct element of the wildfire environment (Fig. 3). We associate each domain with a specific set of variables to describe its specific conditions and properties.

Atmosphere. The atmosphere domain is a three-dimensional space that defines the atmospheric variables such as temperature T_a, light exposure L, water vapor q_v, smoke q_s, and the wind field u. Together, these factors set the overall climatic conditions influencing the fire behavior, including its propagation and intensity. Additionally, it is within this space that smoke disperses and wind influences the direction and speed of the wildfire. We compute local light exposure by performing a single step of shadow propagation based on pyramid-shaped shadow cones [Palubicki et al. 2009]. The shadow cones are extended from each module position to update light exposure values of grid cells within that volume, which allow us to approximate light conditions for the whole scene.

Boundary Fuel Layer - Grass. This is a two-dimensional layer representing the grassy ground cover. For the grass layer we define the grass biomass ϖ_g, its temperature T_g, and moisture content W_g to describe how easily grass may ignite and how rapidly the fire will spread at ground level. Users may specify the type of grass present in the scene by defining species-specific climatic adaptation parameters for temperature T_A, humidity P_A, and light L_A.

Boundary Fuel Layer - Fine Fuel. The fine fuel layer is another two-dimensional layer, which represents smaller fuels such as twigs, leaves, and other loose organic material. The variables defined within this layer include the fine fuel biomass ϖ_f, its temperature T_f, and moisture content W_f. Our method specifies a number of parameters determining the amount and distribution of fine fuel. Fine fuels, due to their size and surface-to-volume ratio, are typically the first to ignite and can significantly influence the fire's spread.

Boundary Fuel Layer - Duff. The duff layer, also a 2D domain, represents the layer of decomposing organic material found beneath the litter of leaves and twigs. This layer defines the duff biomass ϖ_d, its temperature T_d, and moisture content W_d. The properties of the duff layer can impact the smoldering and the underground spread of the wildfire, as well as its duration.

Multi-Domain Mapping. Co-locating the 2D domains of grass, duff, and fine fuel with the 3D domain of the atmosphere mathematically requires mapping between the respective grids. In the 3D atmosphere domain, a z-coordinate value is associated with each point. This z-coordinate corresponds to the height above the ground level. We place the grass, duff, and fine fuel domains in the atmospheric domain based on their real-world heights. To co-locate these domains, we define a function $z = h(x, y)$ that maps each point in the 2D domain (x, y) to a height z in the 3D domain. This function is defined for each 2D layer. Therefore, we refer to the grass, fine fuel, and duff domains as the boundary fuel layer domains – the interface between ground and atmosphere. Interactions between the layers can then be calculated based on the spatial proximity and properties at each co-located point.

5.3 Vegetation Model

To represent vegetation we use a vigor-based representation for plants [Makowski et al. 2019]. We employ a hierarchical, discrete graph representation composed of modules and branch segments to represent plants. A module $\mathcal{M}$ is composed of a set of connected branch segments where each branch segment is defined by a truncated cone. It can be described by a graph $G_{\mathcal{M}}$. Each module $\mathcal{M}$ is defined by a set of attributes comprised of moisture W, mass M, light flux Q, and vigor V. At the next higher scale of the hierarchy a plant $\mathcal{P}$ is defined by a graph $H_{\mathcal{P}}$ as a set of connected modules. In addition, each plant also has a number of plant type attributes which define various species dependent traits relevant to wildfire modeling. Specifically, each plant is defined by average fine fuel production φ_f, fine fuel spread σ_f, temperature adaptation T_A, humidity adaptation P_A, moisture production ψ, and transpiration rate κ_p. A full list of module and plant type parameters can be found in the Appendix (A.3). This multi-scale graph representation is used to generate realistic plant geometry (Fig. 18, Appendix A.1).

We propose a method to compute fuel moisture values W for each module M of a plant $\mathcal{P}$ based on four steps: computing plant environmental adaptation, approximating local light conditions, distributing vigor to modules based on light conditions, and computing time-varying fuel moisture based on module vigor (Fig. 3b-d). For model details we refer to Makowski et al. [2019].

Once we have computed vigor V for all modules, we compute their fuel moisture. We posit that branches exhibiting higher vigor, indicative of healthier and more hydrated vegetation, inherently possess higher moisture content, making them less readily combustible. Conversely, branches with lower vigor, suggesting weakened or dehydrated vegetation, have reduced moisture content, making them more prone to ignition and combustion. We compute the initial fuel moisture W of module $\mathcal{M}$ using a sum of softplus and sigmoid logistic functions:

$$W_{\mathcal{M}}(V_{\mathcal{M}}, M_{\mathcal{M}}) = \log(1 + e^{V_{\mathcal{M}}}) \cdot \psi \cdot M_{\mathcal{M}} + W_{min} \cdot \frac{1}{1 + e^{-V_{\mathcal{M}}}}, \quad (1)$$

where ψ is a coefficient expressing species dependent moisture content, W_{min} defines a minimum fuel moisture value for a given plant type, and $M_{\mathcal{M}}$ is the total mass of a module. We define a starting moisture value for modules and calculate their changes over time that may result from transpiration due to heat:

$$\frac{dW_{\mathcal{M}}}{dt} = \kappa_w^m(T_{\mathcal{M}}) \cdot A, \quad (2)$$

where κ_w^m denotes an evaporation function for plants and A is the surface area of module $\mathcal{M}$. κ_w^m follows the idea of Arrhenius reaction rate but is modeled by a smoothstep function ($S_{a,b} : x \mapsto 3\bar{x}^2 - 2\bar{x}^3$ where $\bar{x} = max(0, min(1, (x - a)/(b - a)))$). This means that κ_w^m,

$$\kappa_w^m(T_{\mathcal{M}}) = S_{T_0^m, T_1^m}(T_{\mathcal{M}}) \quad (3)$$

in our model is described by a sigmoid-like function for computational efficiency reasons. Please note that in contrast to Hädrich et al. [2021] we simulate the evapotranspiration of water prior to combustion. This significantly increases the realism of our model as organic material has to dry up first before it can ignite. We also take into account the evaporation of water from the soil by considering the temperature of the duff layer

$$\frac{\partial q_w}{\partial t} = \Delta q_w - \kappa_w^d(T_d) q_w, \quad (4)$$

where Δq_w represents water diffusion in the soil and where κ_w^d denotes an evaporation function. κ_w^d follows the idea of Arrhenius reaction rate but is modeled in our case by a smoothstep function:

$$\kappa_w^d(T_d) = S_{T_0^d, T_1^d}(T_d) \quad (5)$$

The terms $\kappa_w^m(T_{\mathcal{M}})A$ from Eq. (2) and $\kappa_w^d(T_d)q_w$ from Eq. (4) have to be accounted for when describing the rate of change of vapor q_v of the atmospheric model [Hädrich et al. 2021]. In summary, our vegetation model enables a detailed representation of fuel moisture by taking into account light exposure, vigor of branches and the overall climatic adaptation of a plant to a particular region, as well as the evapotranspiration of plants and soil during a wildfire.

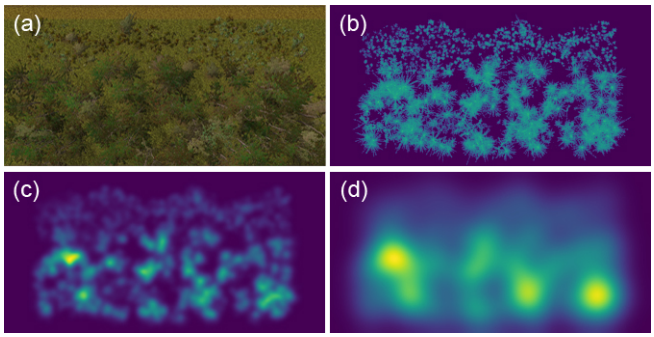

Fig. 4. Stages of fine fuel map computation: top-down view of the forest edge scene (a). A colormap representation of plant modules indicating distinct plants and their structure within the ecosystem (b). Fine fuel map generated using a smaller value of the parameter σ_f, depicting how fuel is distributed closely around individual plants (c). Fine fuel map computed with a larger σ_f value, demonstrating a broader spread of fine fuel around each plant (d).

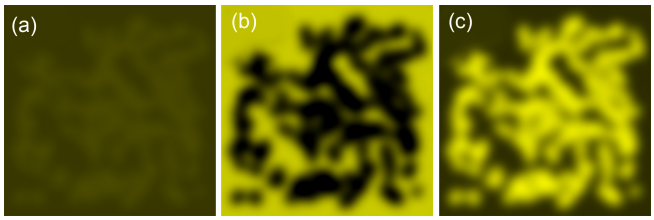

Fig. 5. An example arrangement of duff (a), grass (b), and fine fuel (c), generated using our boundary fuel model. Grass is avoiding the regions where shrubs are located (dark spots), whereas duff and fine fuel are found more readily around the locations of shrubs.

5.4 Boundary Fuel Model

Our boundary fuel model is defined by a layer-based representation for grass, fine fuel, and duff. Together, these layers capture the complexity of surface fuels typically present in wildfire-prone environments. The grass layer represents the highly reactive fuels that often serve as a catalyst for fire initiation and rapid spread. This layer is characterized by its low moisture content and high surface-area-to-volume ratio, leading to quick ignition and combustion. Fine fuels, such as small twigs and leaves, constitute the second layer. These fuels have a slower reaction time due to their larger size compared to grasses but contribute significantly to the heat release rate during active burning [Bishop 2007]. Lastly, the duff layer represents the organic material accumulated on the forest floor, including decomposed leaves, branches, and other detritus. This layer burns slowly and can smolder for extended periods of time, contributing to the duration of the fire and serving as a heat source for reignition.

All these layers with different combustion properties may interact with each other by exchanging heat. Including them is necessary to describe surface fires and progressions of wildfires from surface to canopy fires. Fine fuel and duff are distributed in proximity to larger vegetation, whereas grass avoids shaded regions. A simplification of the three fuel layers into a single surface layer would neglect these spatial patterns and their specific combustion and heat transfer properties.

In our mathematical model we represent grasses as a concentration of biomass on a 2D grid. This model is specifically designed to define a plausible grass cover based on light availability, temperature, and soil water availability. Each grid cell in the model is assigned a biomass value B_g:

$$B_g(x,y) = \frac{\mathcal{N}_T(T_a)\cdot\mathcal{N}_L(L)\cdot\mathcal{N}_P(q_w)}{\mathcal{N}_T(T_A)\cdot\mathcal{N}_L(L_A)\cdot\mathcal{N}_P(P_A)}\cdot\varpi_g\,, \tag{6}$$

where x and y describe a position in the 2D map, ϖ_g is the biomass of the type of grass under ideal conditions, $\mathcal{N}_T(\cdot)$, $\mathcal{N}_L(\cdot)$ and $\mathcal{N}_P(\cdot)$ denote the normal distributions of temperature, light and soil water. We sample the light exposure L and the temperature T_a at the grid cell of the atmosphere space associated with the corresponding grass space cell (x,y). A distinctive feature of this model is the ability to express different grass species by allowing users to specify values of environmental adaptation parameters. These parameters encapsulate the specific adaptive traits of grass species in response to environmental variables, allowing for the simulation of various grass types under diverse climatic conditions.

Duff map B_d and fine fuel map B_f are obtained by sampling all plants associated with the wildfire scene. The computation of the fine fuel amount is based on the total biomass of all plant modules. Each module's contribution to the fine fuel layer is calculated based on its biomass. This biomass is processed through a kernel function, referred to as the fine fuel kernel G_f which transforms the 3D plant module biomass distribution into a 2D map of fine fuel amount,

$$G_f(\mathcal{M},x,y) = \frac{\varpi_f}{2\pi\sigma_f^2}e^{-\frac{(x-x_\mathcal{M})^2+(y-y_\mathcal{M})^2}{2\sigma_f^2}}\cdot M_\mathcal{M}\cdot\varphi_f\,, \tag{7}$$

where $x_\mathcal{M}$ and $y_\mathcal{M}$ are the position of a module in 3D space, ϖ_f a global fine fuel biomass scaling coefficient, σ_f is the standard deviation of the Gaussian distribution which determines the spread or width of the Gaussian function, $M_\mathcal{M}$ the biomass of the module of a plant, and φ_f a coefficient that describes how prone a given plant species is to distribute fine fuel. The fine fuel kernel function accounts for the dispersal and deposition patterns of fine fuels, capturing the effect of plant structure on the distribution of these fuels. In Fig. 4 we show two example fine fuel maps (c, d) computed from an initial scene (a) and a visualization of the modules (b). Varying σ_f values allows to control the range of fine fuel dispersal. Similarly, the duff layer is computed from the 3D modules, but the translation considers the accumulation and decomposition patterns dependent on humidity:

$$G_d(\mathcal{M},x,y) = \frac{\varpi_d}{2\pi\sigma_f^2}e^{-\frac{(x-x_\mathcal{M})^2+(y-y_\mathcal{M})^2}{2\sigma_f^2}}\cdot M_\mathcal{M}\cdot\varphi_f\cdot\mu_d(q_w)\,, \tag{8}$$

$$\mu_d(q_w) = e^{-\frac{1}{2}\left(\frac{q_w-\mu_d^{opt}}{\sigma_d}\right)^2}, \tag{9}$$

where the duff kernel function is defined analogously to the fine fuel kernel function but additionally depends on a moisture function μ_d derived from soil water q_w, an optimal moisture value for decomposition μ_d^{opt}, and a term controlling the spread of the bell-shaped curve σ_d. The closer the soil water amount is to the optimal moisture value the faster fine fuel is transformed to duff. We obtain 2D maps representing the biomass of fine fuel and duff by accumulating the kernel functions for all plants:

$$B_f(x,y) = \sum_\mathcal{P}\sum_{\mathcal{M}\in\mathcal{P}} G_f(\mathcal{M},x,y), \tag{10}$$

$$B_d(x,y) = \sum_\mathcal{P}\sum_{\mathcal{M}\in\mathcal{P}} G_d(\mathcal{M},x,y). \tag{11}$$

By using this approach, our model provides a spatially explicit representation of the boundary fuels. The computation of grass, fine fuel, and duff moisture W_g, W_f, W_d is achieved by linearly scaling soil water q_w with coefficients ψ_g, ψ_f, ψ_d expressing layer-specific moisture control (e.g., $W_g = \psi_g \cdot q_w$). The rate of change of the boundary fuel layer biomass and moisture is then defined by:

$$\frac{\mathrm{d}B_b}{\mathrm{d}t} = -k(T_b,W_b),\ \frac{\mathrm{d}W_b}{\mathrm{d}t} = -k_w(T_b,W_b)\sqrt{B_b}, \tag{12}$$

where the index b indicates any of the three boundary fuel types and T_b the temperature (see Eqs. 18, 19, 20). An example rendering of the 2D maps after considering the contribution of all modules is shown in Fig. 5. In this scene grass is avoiding the locations of shrubs due to lower light exposure values (dark spots, Fig. 5b), while duff and fine fuel are arranged in some proximity of the shrubs according to the Gaussian kernel calculations (light color, Fig. 5a, c).

5.5 Combustion

The main mechanism driving a wildfire is the combustion of wood and other organic matter that act as fuel. Combustion is a chemical reaction that occurs between a fuel and an oxidizing agent, typically oxygen, resulting in the production of heat, light, and various reaction products such as water and carbon dioxide. Our model is following a simpler one-step combustion approach (e.g. [Galgano and Di Blasi 2005]). Specifically, we extend the combustion model of Hädrich et al. [2021] by including vapor in the combustion process. Organic material is decomposed into char, flammable gases (fuel), and vapor i.e.,

$$\text{Organic Material} + \text{Heat} \rightarrow \text{Fuel} + \text{Char} + \text{Vapor}\,.$$

The addition of vapor into the combustion component of our model allows us to distinguish the combustion of moist vegetation (e.g. in a rainforest), from drier vegetation (e.g. in a savannah). The removal of moisture from vegetation due to heat precedes the actual burning of the vegetation and therefore can delay the onset of a live fire. Without the modeling of heat-driven evaporation all vegetation would start burning at the same time and we could not express wildfires for different biomes in a plausible manner.

Additionally, we extend the rate of mass change introduced in Pirk et al. [2017] $\mathrm{d}M/\mathrm{d}t$ to account for fuel moisture and water vapor which can be described by

$$\frac{\mathrm{d}M}{\mathrm{d}t} + k(T_\mathcal{M},W_\mathcal{M},u)\,c\,A = 0\,, \tag{13}$$

$$k(T_\mathcal{M},W_\mathcal{M},u) = \eta(u)\cdot S_{T_0,T_1}(T_\mathcal{M})\cdot S_{W_0,W_1}(W_\mathcal{M}), \tag{14}$$

$$\eta(u) = 1 + (\eta_{\max}-1)\,S_{0,u_{\text{ref}}}(u)\,, \tag{15}$$

where k denotes the reaction rate of the combusting fuel which is obtained from the temperature of the module $T_\mathcal{M}$, the total moisture of module $W_\mathcal{M}$, and wind speed u. The dimensionless char insulation parameter is denoted by c and the pyrolyzing front area by A. Both, c

and A depend on the tree geometry and vary during the combustion process. Please see Hädrich et al. [2021] for a detailed description. In contrast, in our model we extend the description of the reaction rate to also take into account fuel moisture. In reality, wood or other organic fuels with high moisture content do not combust as easily as dry fuels, and the moisture must be evaporated before combustion can proceed, which requires additional energy and hence slows down the reaction. Consequently, this is an important extension to increase the realism of wildfire modeling. However, we keep the sigmoid-like relationship as already introduced in Sec. 5.3 (Eq. 3) to ensure an efficient computation (compared to using an exponential function). Variable η describes the impact of wind on the reaction rate, where we assume that strong winds can increase the reaction rate. We use the definition of η where u_{ref} denotes a reference wind speed for maximum boost.

5.6 Heat Transfer

In our model, wildfires are defined by the complex interplay of heat transfer processes across multiple spatial domains. The 3D atmospheric domain represents the air above the ground and is subject to heat transfer processes such as conduction, convection, and radiation. We define a time-dependent vector-valued velocity field $\boldsymbol{u} : (\boldsymbol{x}, t) \mapsto \boldsymbol{u}(\boldsymbol{x}, t)$ which for given time $t \in \mathbb{R}^{\geq 0}$ and position $\boldsymbol{x} \in \mathbb{R}^3$ returns the corresponding local flow $\boldsymbol{u}(\boldsymbol{x}, t) \in \mathbb{R}^3$. The temporal evolution of $\boldsymbol{u}$ follows Hädrich et al. [2021] and defines drag as well as buoyancy forces. We define temperature as a scalar field returning the corresponding temperatures T_a at times $t \in \mathbb{R}^{\geq 0}$ at positions $\boldsymbol{x} \in \mathbb{R}^3$:

$$\begin{aligned}\frac{\partial T_a}{\partial t} + \boldsymbol{u} \cdot \nabla T_a = \alpha \nabla^2 T_a - \gamma(T_a^4 - T_{\text{amb}}^4) - \tau \frac{\mathrm{d}M_s}{\mathrm{d}t} \\ - K_{ga}(T_a - T_g) - K_{fa}(T_a - T_f)\,,\end{aligned} \tag{16}$$

where the terms $K_{ij}(T_j - T_i)$ represent the heat flux from domain j to domain i, K_{ij} is the thermal conductivity at the interface between the domains, and γ denotes the radiative cooling coefficient introduced by Nguyen et al. [2002]. In our model, only the grass and fine fuel layers transfer heat into the atmosphere as they are assumed to be in direct contact with air. The duff layer does not transfer heat to the atmosphere as it represents the soil layer which is not directly exposed to the air and is therefore omitted from Eq. 16. Please note that in Hädrich et al. [2021] the boundary fuel domains are not included. The temporal temperature change of a certain fluid parcel, as it flows along the trajectory of the wind, is described by a diffusion component with intensity α, and an ambient cooling component with the radiative cooling term γ involving a fixed ambient temperature T_{amb}. Whereas, K_{ga} denotes the heat conductivity between grass and the atmosphere and T_g is the grass temperature. M_s denotes the mass of grid cell, and is defined as the weighted sum of vegetation modules's mass that overlap this grid cell. The water content W_s in each grid cell is similarly defined.

Vegetation, which serves as the fuel source in wildfires, is represented using a graph-based model, with nodes representing branch modules and edges connecting them. Therefore, in addition to the environmental temperature field T_a, we introduce a module temperature function $T_{\mathcal{M}}(M, t)$ which for given time $t \in \mathbb{R}^{\geq 0}$ and module $\mathcal{M}$ returns the module's surface temperature. Heat transfer of modules is described as heat conduction between modules and radiative heat exchange with the atmosphere:

$$\frac{\partial T_{\mathcal{M}}}{\partial t} = \alpha_m \nabla^2 T_{\mathcal{M}} + b(T_a - T_{\mathcal{M}})\,, \tag{17}$$

where α_m and b denote diffusion and temperature coefficients.

Heat transfer in the boundary fuel domains is modeled by two-dimensional heat conduction equations, capturing the transfer of heat within and between these layers. These equations are coupled with the 3D atmosphere domain through boundary conditions that represent heat exchange between the ground layers and the atmosphere:

$$\frac{\partial T_g}{\partial t} = D_g \nabla^2 T_g + K_{ga}(T_a - T_g) + K_{gf}(T_f - T_g) + K_{gd}(T_d - T_g)\,, \tag{18}$$

$$\begin{aligned}\frac{\partial T_f}{\partial t} = D_f \nabla^2 T_f + K_{fa}(T_a - T_f) + K_{fg}(T_g - T_f) \\ + K_{fd}(T_d - T_f)\end{aligned}, \tag{19}$$

$$\frac{\partial T_d}{\partial t} = D_d \nabla^2 T_d + K_{df}(T_f - T_d) + K_{dg}(T_g - T_d)\,, \tag{20}$$

The diffusion terms in Eqs. (18 - 20) describe heat conduction inside each boundary fuel layer. Heat conduction is fastest in grass, then fine fuels and slowest in duff [Bishop 2007]. The remaining terms in the equations express heat transfer between the boundary fuel layers. Specifically, we assume that the rate of change of temperature in the grass layer and fine fuel layer depend on heat transfer between air and the other boundary fuel layers, but the duff layer exchanges heat only with the other boundary fuel layers. This means, that in our model, flammable grass or fine fuel must be present for a smoldering ground fire to initiate a wildfire as it does not directly transfer heat to other vegetation or air. In reality, such ground fires have been observed in tundras where they can stay active for months before initiating a surface fire that combusts aboveground vegetation [Innes 2013].

5.7 Sparks and Embers

During wood combustion micro and macro cracks appear on the charred wood surface as a result of different thermal expansion of wood and char which can lead to the release of embers. In real wildfires, sparks and embers can lead to sudden new fires, even at distant locations from the main fireline. Consequently, understanding how firebrands are generated and transported is of paramount importance for firefighting. Due to the complexity of the phenomena involved in the event of a wildfire, such as heat transfer, fluid dynamics, combustion, and structural failure, it has yet to be fully understood. A wildfire model that does not account for the effects of embers would lead to fireline progressions which are predictable and have simpler shapes.

To include the effects of embers for wildfires we need to establish the rate of their generation. Adusumilli et al. [2021] have shown that the particles released per kilogram of fuel consumed are around 10^3 for different species. We include this observation in our model by assuming that the number of particles released is proportional

to the amount of burnt fuel, i.e.,

$$\frac{\mathrm{d}N_e}{\mathrm{d}t} = c_e \frac{\mathrm{d}M}{\mathrm{d}t}\,, \tag{21}$$

in which c_e is a species-specific constant and N_e is the ember release rate occurring during the combustion in every tree module. In addition to the ember generation rate, it is important for an ember model to describe realistic geometric properties of embers due to their strong influence on transport and ignition phenomena. Therefore, we consider the statistical work made by Tohidi et al. [2015] which shows that the ember surface area A_e follows a logarithmic normal distribution $\mathrm{LogNormal}(\mu_{\log}, \sigma_{\log})$ with logarithmic mean and standard deviation

$$\mu_{\log} = \log \frac{\mu^2}{\sqrt{\mu^2+\sigma^2}}\,, \quad \sigma^2_{\log} = \log\left(1+\frac{\sigma^2}{\mu^2}\right), \tag{22}$$

in which μ and σ are calculated from the experimental data collected by Manzello et al. [2009]. In order to estimate the ember mass, we use the ember surface area: $m_e \approx A_e^{3/2}$.

Ember transport. The firebrands are defined as 3D particles with the attributes position (same as the module position), velocity, and acceleration. To update the particle attributes we use the drag forces generated by the fire plume and wind, the embers' weight, but neglected lift forces due to the small velocity gradients around the embers. The drag force was estimated using a correlation proposed by Schiller and Naumann [1935] to calculate the drag coefficient.

Combustion and heat transfer by embers. To express combustion and heat transfer of embers we define additional particle attributes: temperature, size, and age. Our ember combustion is simpler compared to the module combustion given by Eqs. (13- 15). We neglect the changes in moisture content for embers assuming they are dry and hot objects with approximately constant moisture values throughout our simulation. The rate of change of ember mass is given by:

$$\frac{\mathrm{d}m_e}{\mathrm{d}t} + k(T_e, u_{\mathrm{rel}})\, c\, A_e = 0\,, \tag{23}$$

where A_e denotes the ember surface area, u_{rel} the speed difference between ember and wind, and T_e the ember temperature. Moreover, according to Stefan-Boltzmann and Newton cooling laws, we estimated the ember temperature change by

$$m_e C p_e \frac{\partial T_e}{\partial t} = \sigma A_e (T^4_{\mathrm{amb}} - T^4_e) + h A_e (T_a - T_e) - \Delta H_c \frac{\mathrm{d}m_e}{\mathrm{d}t}\,. \tag{24}$$

The convective coefficient h is given by the correlation proposed by Whitaker [1972] and ΔH_c denotes the combustion heat rate.

Fire spot ignition by embers. To model spot ignition we considered the research of various authors, including Babrauskas [2003] and Jones [1993] [1994], where they proposed a theory developed by Gol'dshleger et al. [1973]. Gol'dshleger's theory, called the hot spot theory, involves the analytical determination of the critical radius of hot particles with a fixed temperature to ignite explosive fuels. We selected an analytical solution of heat transfer between embers and other vegetation over an integration with our numerical solution of heat transfer. A numerical integration would require to significantly reduce the size of time steps to account for the rapid heat transfer between hot embers and unignited vegetation. This design choice results in a more approximate description of the phenomenon, but

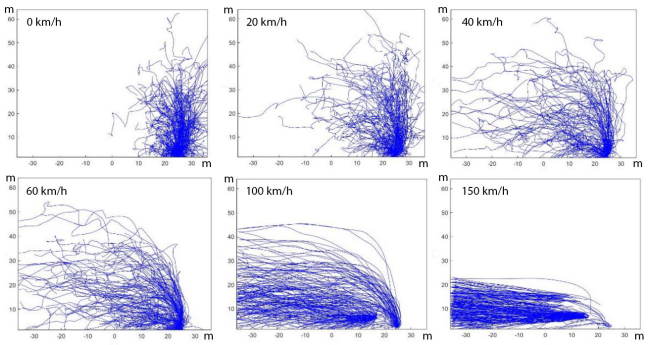

Fig. 6. 100 Firebrand trajectories depicted as blue lines for various vertical wind profiles of varying speeds ranging from 0, 20, 40, 60, 100, and 150 km/h. The trajectories are more random with lower velocities compared to high wind velocities, but at higher wind speeds the embers are carried a longer distance. The range of how far the embers travel is given in meters (m).

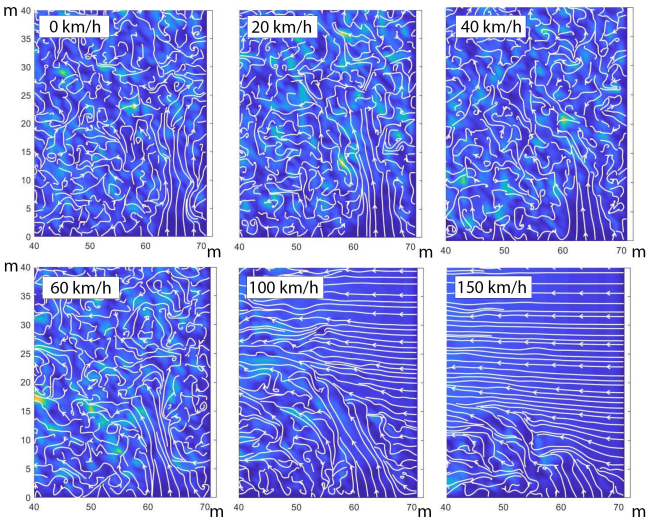

Fig. 7. Stream plots of the wind field for the simulation results shown in Figure 6 with varying speeds ranging from 0, 20, 40, 60, 100, and 150 km/h. The color map jet indicates the speed of the wind field. The stream plots indicate a higher updraft at the position of the fire at lower wind velocities which explains the more erratic trajectories of embers. For both axes the range of how far the embers travel is given in meters (m).

allows us to maintain interactive simulation rates. Specifically, we employ an analytical solution based on the model proposed by Hadden et al. [2011], who demonstrated experimentally that the hot spot ignition theory can be a reliable qualitative indicator for ignition of grass beds by embers. When the ember intersects a module or the bottom grid layer of our simulation domain, we model the grass ignition in a grass layer cell by estimating the minimum particle radius necessary for ignition as follows

$$r_{cr} = \delta_{cr} \sqrt{\frac{K_{gg}}{\rho_g A_g \Delta H_g} \frac{R T_e^2}{E} \exp\left(\frac{E}{R T_e}\right)}\,. \tag{25}$$

ALGORITHM 1: Wildfire simulation preparation.

Input: Digital elevation model of the terrain, multi-scale plant graphs, atmosphere data structure, soil map.
Output: Fuel moisture content of vegetation, 2D spatial maps of grass, fine fuel, and duff distribution.

1 Approximate local light conditions L (Sec. 5.2)
2 **Compute the fuel moisture content for each plant module:**
3 | **for each** plant $\mathcal{P}$ in vegetation **do**
4 | | Compute plant environmental adaptation o using Eq. (26)
5 | | Distribute light flux Q through the plant graph H using Eq. (27)
6 | | Distribute vigor flux V through the plant graph H using Eq. (30)
7 | | **for each** module $\mathcal{M} \in \mathcal{P}$ **do**
8 | | | Compute fuel moisture $W_{\mathcal{M}}$ based on vigor $V_{\mathcal{M}}$ using Eq. (1)
9 | | **end**
10 | **end**
11 **Compute 2D spatial maps for grass, fine fuel, and duff:**
12 | For each cell in the grid, compute biomass B_g, B_f, B_d as per Eqs. 6, 10, 11
13 **end**

ALGORITHM 2: Numerical procedure of our simulator.

Input: Current system state.
Output: Updated system state.

1 **for each** module $\mathcal{M} \in \bigcup \mathcal{P}$ **do**
2 | Update mass $M_{\mathcal{M}}$ according to Eq. (13).
3 | Update moisture $W_{\mathcal{M}}$ according to Eq. (2).
4 | Generate firebrands according to Eq. (21) and Eq. (22).
5 | Perform radii update according to Eq. (Hädrich et al. [2021]).
6 | Update temperature $T_{\mathcal{M}}$ according to Eq. (17).
7 **end**
8 **for each** firebrand **do**
9 | Update mass m_e according to Eq. (23).
10 | Update temperature T_e according to Eq. (24).
11 | Update position and velocity by taking drag into account.
12 | Check intersection with modules and bottom boundary layer.
13 | Compute ignition event according to Eq. (25).
14 **end**
15 **for each** grid cell $\boldsymbol{x}$ in fuel layers B_g, B_f, B_d **do**
16 | Update masses M_g,M_f,M_d according to Eq. (13).
17 | Update moisture W_g,W_f,W_d according to Eq. (12)
18 | Update temperatures T_g, T_f, T_d according to Eqs. 18, 19, 20.
19 **end**
20 **for each** cell $\boldsymbol{x}$ in atmospheric grid **do**
21 | Update $M_s := M_s(\boldsymbol{x}, \boldsymbol{t})$ and $W_s := W_s(\boldsymbol{x}, \boldsymbol{t})$ as described in Section 5.6.
22 | Update temperature T_a according to Eq. (16).
23 **end**
24 Update drag forces $\boldsymbol{f}_d$ and buoyancy force $\boldsymbol{b}$ according to Hädrich et al. [2021].
25 Update q_v, q_s, and $\boldsymbol{u}$ according to Hädrich et al. [2021] and Sec. 5.3 including vorticity confinement with intensity ϵ, the advection of $\boldsymbol{u}$ is upgraded to MacCormack method [Selle et al. 2008] (advection of other scalars is still solved with Semi-Lagrange but their back-trace operations are upgraded to RK-2).
26 Update q_w according to Eq. (4).
27 **for each** module $\mathcal{M} \in \bigcup \mathcal{P}$ **do**
28 | **if** $M_{\mathcal{M}} = 0$ **then** $\mathcal{P} \leftarrow \mathcal{P} \setminus (\{\mathcal{M}\} \cup \text{descendants}(\mathcal{M}))$
29 **end**

where δ_{cr} denotes the Frank-Kamenetskii hot spot parameter for ignition (Appendix A.2), k_{gg} the grass thermal conductivity, A a grass pre-exponential factor, E the activation energy, R the universal gas constant, and ΔH_g the grass combustion heat. In case the ember radius is greater than the minimum particle radius for ignition r_{cr}, we raise the temperature of the grass layer to T_1, which is the temperature of combustion. If the ember does not have enough energy to start a new fire, it is discarded. It is worth noting that, like in real wildfires, the ignition of new fire spots in cells is not a sufficient condition to start a fire. New fires will only start in cells where the heat transfer from grass layers to wind and the environment does not suffocate the new fire.

Figure 6 shows example trajectories of our ember model. At low wind velocities the trajectories are quite random leading (a-c) to more unpredictable migration of firebrands compared to the experiments with higher wind velocities (d-f). This can result in a more chaotic shape of the fire front (Figure 14 i-l). The stream plots in Figure 7 expose the shape of the fire plume (at location 60m - 70m) which is the cause of the updraft carrying the firebrands into a higher altitude. Please also note the more turbulent wind field contributing to the random ember trajectories at lower wind velocities.

6 IMPLEMENTATION

We implemented our framework with C++ and CUDA. To facilitate the visualization of fire, we use volume ray casting [Pharr et al. 2016], implemented with OpenGL and GLSL. This process simulates the behavior of light rays as they traverse the volume. Dynamic handling of tree geometries and leaves is accomplished within geometry shaders. This real-time visualization approach enables interactive exploration of our simulations.

In Algorithm 1 we show how to calculate moisture content and to create 2D fuel maps. First, we approximate local light conditions L (Line 1) to affect vegetation health and fuel availability. We then compute the fuel moisture content. For each plant $\mathcal{P}$ (Line 3), we calculate its environmental adaptation o (Line 4) using Eq. (26), distributes light flux Q across the plant graph H (Line 5) via Eq. (27), and does the same for vigor flux V (Line 6) with Eq. (30). Each module $\mathcal{M}$'s fuel moisture $W_{\mathcal{M}}$ is calculated (Line 8) using Eq. (1) based on vigor $V_{\mathcal{M}}$. In the second part (Lines 11-12), we create 2D maps of grass, fine fuel, and duff. We calculate biomass layers B_g, B_f, B_d per grid cell (Line 12) using Eqs. 6, 10, 11. Required inputs are a terrain model, plant graphs, atmosphere data, and soil map. The outputs are the moisture content and 2D fuel maps, preparing the system for wildfire simulation.

In Algorithm 2 we show how to perform the numerical simulations to update the system state. For each module $\mathcal{M}$ in the system (Line 1), we update the mass M (Line 2) following Eq. (13). The moisture W is then updated (Line 3) via Eq. (2), and radii are adjusted according to Hädrich et al. (Line 5). Temperature $T_{\mathcal{M}}$ updates then follow Eq. (17) (Line 6). Next, for each firebrand we update

their mass, temperature, position, velocity, and check for potential ignition with vegetation (Lines 9-13). Subsequently, for each grid cell in fuel layers B_g, B_f, B_d (Line 15), we update masses M_g,M_f,M_d (Line 16) and moisture W_g,W_f,W_d (Line 17) similarly to Eq. (13) and Eq. (2). Then, we update temperatures T_g, T_f, T_d (Line 18) according to Eqs. 18, 19, 20. Next, for each cell in the atmospheric grid (Line 20), we update M_s and W_s (Line 21) as detailed in Section 5.6. We then adjust temperature T_a (Line 22) according to Eq. (16). Then, we modify drag forces $\boldsymbol{f}_d$ and buoyancy force $\boldsymbol{b}$ (Line 24). Further, we update q_v, q_s, and $\boldsymbol{u}$ according to Hädrich et al., incorporating vorticity confinement with intensity ϵ and MacCormack method for $\boldsymbol{u}$'s advection (Line 25). We then proceed to update q_w (Line 26) based on Eq. (4). In the last loop, if a module $\mathcal{M}$'s mass becomes zero, the module and its descendants are removed from the proper plant $\mathcal{P}$ (Line 28). This procedure operates on the current system state to generate an updated system state.

6.1 Numerical procedure

In the *Fire in Paradise* framework [Hädrich et al. 2021], the authors adopted the semi-Lagrangian scheme from the influential paper by Stam [1999] to solve the advection term of the Navier-Stokes equation. This approach, while unconditionally stable, has been recognized to lead to significant numerical diffusion, a limitation that we aimed to overcome. To this end, we employ the unconditionally stable MacCormack scheme [Selle et al. 2008], which has been shown to not only effectively reduce numerical diffusion but also to achieve second-order accuracy, making it a superior choice for our purposes. For the ember transport we use the forward Euler method.

Additionally, we made enhancements to the back trace operations of the advection terms of all related equations, including the Navier-Stokes equation. To increase the precision of these operations, we implemented the second-order Runge-Kutta (RK-2) scheme in place of the previous first-order method. This modification is expected to offer improved accuracy and overall performance of our model. By combining these improvements, we aim to deliver a more robust and accurate wildfire simulation.

Fig. 7 exposes the significant amount of turbulence which occurs during our wildfire simulations. These turbulences are absent when solving with the semi-Lagrangian scheme (Figure 19, Appendix A.6). To quantify the difference between the MacCormack and the semi-Lagrangian scheme, we measured the average kinetic energy for each grid point in the domains, which indicates a 19.35% higher turbulence for the MacCormack scheme. This increase in turbulence is a direct consequence of the reduction in numerical diffusion achieved through our enhancements to the advection solution method. Such a result is significant as it allows a more advanced simulation of turbulent phenomena of wildfire simulations.

6.2 Initial Conditions

We set values for physical parameters of our simulations with readily available observational data, such as T_a, or q_w, according to plausible ranges obtained from the literature. Other parameters can be derived from observational data but might be accurate only in certain

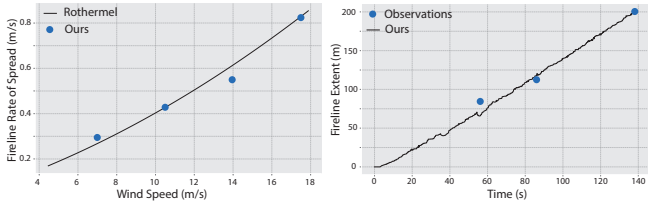

Fig. 8. Left: A comparison of the rate of fire spread of the fireline using Rothermel's model configured for crown fuel [Bishop 2007] (solid line) and our simulation results for four experiments with varying wind speeds. Our simulation results correspond well to Rothermel's model. Right: A comparison of the maximum extent of firelines in our simulation (solid line) to measurements of the controlled burn experiment shown in Fig. 13 at three different time points (blue dots). Our simulation captures accurately the linear progression of the fireline.

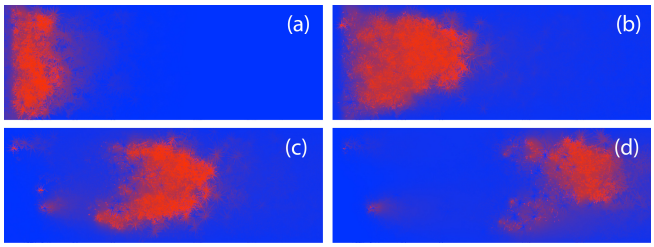

Fig. 9. Heat map of a top down view on a burning forest patch with a wind field directed from left to right. Red color indicates temperature. Letters a-d indicate the temporal progression of the crown fire. The rate of spread of the fireline is approximately constant over time. We use this setup to generate the simulation results of varying wind speeds to compute the data points shown in Fig. 8 (left).

conditions, such as k which can be derived from controlled combustion experiments, W_g which can be derived from soil moisture measurements and known water retention properties of the biomass, or σ_f which can be derived from the observed spread of fine fuels around plants. Obtaining parameter values from observational data can be challenging for variables such as species-specific adaptive parameters like T_A, L_A, and P_A, biological growth parameters such as ϖ_g, kernel functions involved in fuel mapping exemplified by $G_f(x, y)$, and parameters governing thermal and moisture transfer, for instance, K_{ij}. However, we use various research sources to guide our selection of parameter values such as Vanella et al. [2021] to estimate max biomass of fine fuel, grass, duff ϖ_g, ϖ_f, ϖ_d, Bishop [2007] to estimate moisture content per plant species ψ, and Hadden et al. [2011] to set thermal conductivity K_{ij} and combustion heat rate ΔH_c. We also demonstrate that our parameter value selections result in simulations which compare favorable with simulations obtained with the analytical model from Rothermel and a real world burn experiment (Fig.8). For most scenes we use the same initial conditions. A typical list of parameter values used in the simulations we describe here can be found in Appendix A.7.

7 RESULTS

To showcase our wildfire simulation framework we present qualitative results obtained from various experiments. Specifically, we

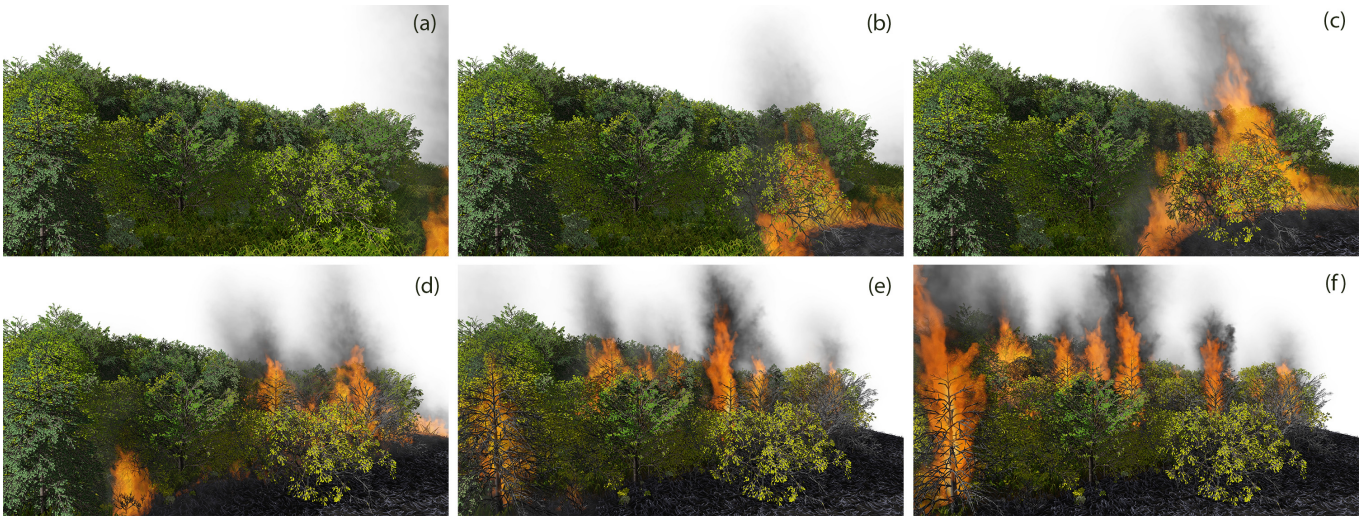

Fig. 10. Progression of wildfire from grassland to forest edge: Initial fire ignition in grassland (a). Fire spreads, establishing as a surface fire (b). Fire reaches the forest edge, with the lower branches beginning to combust (c). Fire's transition from surface to active crown fire begins as it ascends the trees (d). Full transition to active crown fire, showing high-intensity flames within the forest canopy (e). Fire progresses further into the forest, vertical maintaining its status as an active crown fire with flame jets emerging (f).

show that our model can generate known wildfire types, the distinct ranks of wildfires, and wildfires for different types of biomes (Fig. 12). Our model also supports exploring human cultivation factors for wildfire prevention, such as removing trees and shrubs from ecosystems. We validate our simulations with real-world experimental results.

7.1 Types of Wildfires

In our wildfire model offers the capability of simulating a range of wildfire types, from Rank 1 to Rank 6 using the Wildfire Ranking System proposed by the British Columbia Wildfire Services. In our model, wildfires of different ranks can be simulated by adjusting the fuel moisture content of the plant modules. Each rank represents a different level of fire intensity and propagation rate, associated with the fire's interaction with different types of fuels present in the ecosystem. Rank 1, ground fires, typically occur in the organic matter present on the forest floor, known as duff. These fires burn slowly, producing relatively small flames. By increasing the moisture content in the duff layer, our model simulates ground fires. Surface fires, or Rank 2 to 3 fires, involve the combustion of vegetation at the forest floor (leaf litter, and small branches), represented in our model as fine fuel and grass (Fig. 10a,b and Fig. 16a,b). Adjusting the moisture content within these components allows us to control the spread and intensity of surface fires (Table 1). Finally, crown fires, ranks 4 to 6, are the most intense and fast-moving fires, consuming both the surface and canopy fuels (Fig. 10c-e and Fig. 16c-e). The range of different wildfires is simulated in our model by manipulating moisture content within tree modules and the boundary fuel layer. When fuel moisture is low, our model simulates a rapid vertical fire spread, leading to an intuitive control of wildfire severity through fuel moisture parameters.

Fig. 11. Wildfire progression in varying cultivation scenarios. (a) Wildfire simulation in a dense, uncultivated grove with abundant vertical fuel resources in the form of trees of various heights, leading to intense and rapidly spreading wildfires. (b) Illustrates the effects of human cultivation efforts on wildfire behavior, represented by a scenario where medium-sized trees have been removed, resulting in a decrease in fire intensity and spread. (c) Further cultivation effects represented by a scene with minimal shrub presence; the scarcity of vertical fuel resources results primarily in a less severe surface fire.

In Fig. 9 we show a temporal progression of a crown fire in a narrow forest patch as a heat map. Red colors indicate higher temperatures. The fireline progresses from left to right because we apply a wind field in that direction. We computed average velocities for the fireline for different wind speed experiments using our simulation framework. Fig. 8 (left) shows a comparison of four simulation runs with different wind speeds and a corresponding parameterization of Rothermel's model for crown fires [Bishop 2007]. As shown, our simulation runs conform to the Rothermel curve indicating a plausbile simulation of fireline progression with our modeling framework.

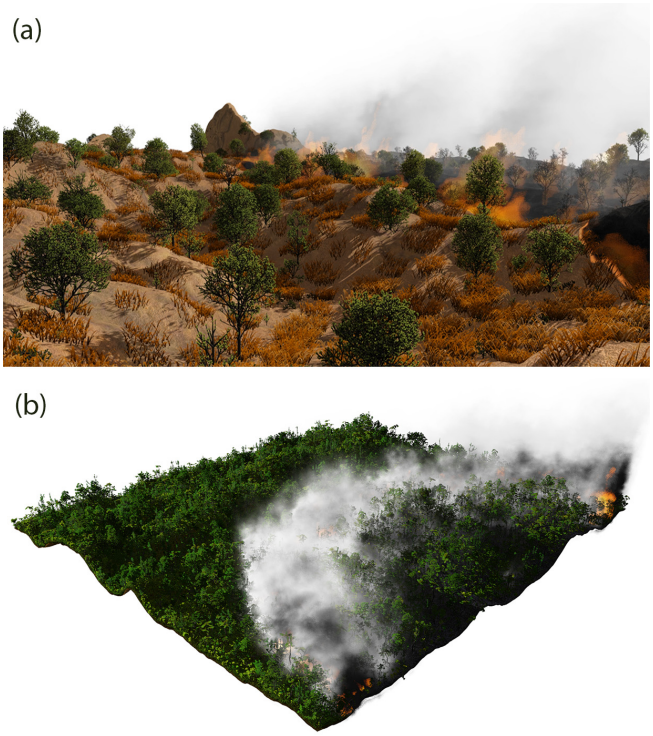

Fig. 12. Renderings showing two different biomes: A close-up of a shrubland fire in the savannah (a) and a wildfire in the jungle characterized by high evaporation (b).

7.2 Human Intervention

By considering different fuel types our wildfire simulation allows assessing the impact of various human intervention methods. An important method is vegetation management to minimize the potential for severe wildfires. In Fig. 11 we show simulation results for different cultivation scenarios and their impact on wildfire progression. In the first scenario (Fig. 11a), the simulation depicts a dense, uncultivated grove with an abundance of vertical fuel resources represented by trees of various heights. As expected, these conditions lead to an intense and rapidly spreading wildfire due to the large amount of fuel. In contrast, Fig. 11b shows a human cultivation scenario, where medium-sized trees have been removed. The results depict a decrease in both the intensity and spread of the simulated wildfires. Lastly, Fig. 11c shows a more severe cutback of the vegetation – even smaller shrubs have been removed. Here, the scarcity of vertical fuel resources results in a less severe surface fire. These outcomes underscore the potential effectiveness of strategic vegetation management for mitigating the impact of wildfires.

7.3 Boundary Fuel Wildfire Simulation

Fireline validation. To validate our wildfire model, we carried out comparisons with real-world experimental results. We prepared a simulation with a uniform grass concentration over a flat terrain of the size 200m x 200m. The fire was initiated along the left edge of the scene following the details provided in [Vanella et al. 2021]. This study involved controlled burns and provides detailed

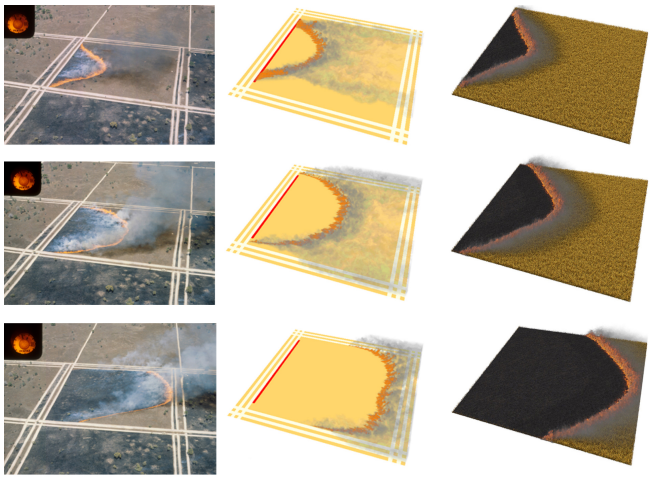

Fig. 13. Photographs of a controlled burn experiment (left), results of a wildfire simulation published by Vanella et al. [2021] (middle), and our simulation results (right). Our simulation captures the main characteristics of the progressing fireline in the controlled burn experiment.

observations and measurements that offer a suitable benchmark for our model. In these experiments, fires were ignited by two field workers with drip torches, who walked in opposite directions along the upwind boundary of the plot. We simulate an identical ignition process in our framework. Our simulated fireline progression shows remarkable similarity with the experimentally observed fire progression documented in the study. The shape, direction, and general characteristics of fire spread in our model replicates the main features of the fireline from the experimental results (Fig. 13). We also quantitatively compared the extent of the fireline to the observations of a controlled burn experiment (Fig. 8, right). The plot shows the close correspondence of our simulation results to real-world measurements of a fireline in three different time points. In Fig. 21 (Appendix A.9) we overlay our simulated fireline (red contour) with the observed measurements (dots, squares, triangles) and the results of the simulation by Vanella et al. [2021] for clarity.

Boundary fuel distribution. In the controlled burn scenario a symmetric fireline progression emerges. However, in reality firelines often show more intricate progression dynamics. The dispersion pattern of fine fuel spots can, for example, instigate a localized retardation in the progression of the fireline, which can lead to an emergent complexity of the wildfire's structure. In Fig. 15 we show a temporal progression of a wildfire initiated at the left side of the scene. An uneven distribution of fine fuel (indicated by greener areas) leads to an uneven fireline advancement. A wildfire in such a fuel environment is characterized by the creation of *fingers* which are extended, narrow protrusions of the fireline that reach further into unburnt areas (Fig. 15a-c). Similarly, the fireline can retract or slow down in areas of lower fuel availability, leading to the formation of *bays* –recesses or indentations in the fireline that represent areas where the fire has not yet or may not reach. This gives the fireline a unique, irregular shape, further enhancing the visual and dynamical realism of the simulation (Fig. 15e). Furthermore, if the

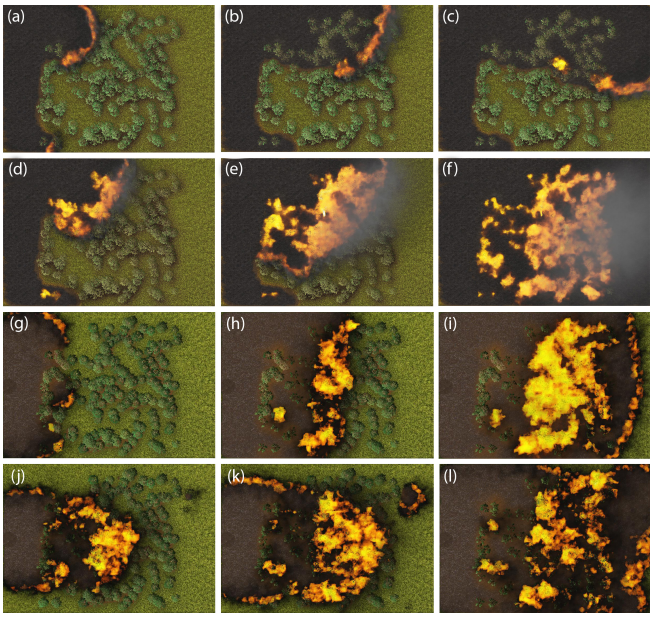

Fig. 14. The initial state of a grassland ecosystem interspersed with moisture-rich shrubs viewed from above without ember model (a). Simulation result showing the progression of the wildfire, which avoids the dense line of shrubs due to their higher fuel moisture content (b). Final state of the wildfire progression showing the protective role of moisture-rich shrubs against fire spread (c). In the row below (d-f), we show the same scene but with lowered fuel moisture values for the shrubs. In this case, the wildfire simulation results in complete conflagration. In (g-i) we show a simulation with the ember model. In this case a new spot fire ahead of the fireline emerges in (g) and leads to a straighter fireline compared to the two top rows. In (j-l) we add wind from left to right which results in new spot fires appearing further away from the fireline (j, k). The interplay between fuel moisture distribution and firebrand simulation leads to complex fireline shapes in our wildfire simulations.

fireline encircles an area of unburnt vegetation, it may result in the creation of *islands*. These are patches of unburnt vegetation surrounded by burnt areas, signifying the heterogeneity in fire propagation due to fine-scale variations in fuel distribution (Fig. 15d).

Fuel moisture effect. A key advantage of our approach is that it allows us to capture the complexities of fireline progression dynamics that account for variable fuel moisture. In particular, the simulation results have demonstrated the crucial role of fuel moisture distribution in modulating the spread and behavior of wildfires. In scenarios where shrubs — which typically contain higher fuel moisture compared to grass — are distributed within a grassland, our simulation shows that they can act as a natural barrier to the progression of fire (Fig. 14a). Specifically, the fireline is observed to navigate around these denser lines of shrubs, selecting paths where the shrub density – and consequently the fuel moisture content – is lower (Fig. 14b, c). This behavior shows that the wildfire is attracted by areas of lower fuel moisture, leading to a more realistic and complex fireline progression pattern. To test the influence of fuel moisture content further, we conducted a second experiment where the fuel moisture content of the shrubs was reduced. The results of this experiment show a less pronounced retardation of the

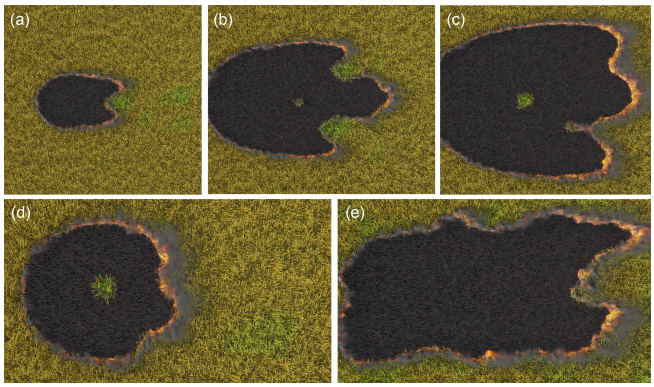

Fig. 15. Anatomical parts of a wildfire. (a): Initial configuration showing the ecosystem with the distribution of fine fuel spots (indicated by greener color). (b): Early stages of fireline progression with local delays evident at fine fuel spots. (c): Intermediate stage of the wildfire, displaying complex progression dynamics including finger formations. (d): Advanced stage, where bay and island formations become apparent due to the localized slowing of the fireline at the fine fuel spots. (e): Final state of the wildfire highlighting the intricate anatomy shaped by the distribution of fine fuel.

fireline progression around the shrubs (Fig. 14d-f). This outcome shows that fuel moisture content plays a significant role in defining the rate and direction of wildfire spread.

Ember Influence and Wind Dynamics. The simulation results depicted in (Fig. 14 g-i) incorporate the ember model. These simulations differ from the previous grassland wildfire due to the emergence of new ignition points that advance the fireline (g, j, k), resulting in a more linear fireline front. This linearization is a direct consequence of embers migrating in the immediate area of the primary fireline and starting auxiliary fires that eventually merge with the main front. Subsequent frames (Fig. 14 j-l) introduce a wind field from the left to right. This interaction leads to ignition points appearing further from the primary fireline, leading to complex shapes of wildfire progression. In Fig. 20 we quantitatively compare the mass loss evolution for the experiments shown in Fig. 14 a-f. The inclusion of embers in our model leads to higher total mass loss (dotted graph) compared to the ablated experiment (solid line) – especially for the scene with higher fuel moisture (blue graphs). Our simulations with the ember model and varying fuel moisture distribution showcase the unpredictable nature of wildfire spread, emphasizing the need for detailed, spatial models in wildfire research.

8 DISCUSSION AND LIMITATIONS

We have presented a method for simulating realistic wildfires across a variety of scenarios. The key novelty of our approach is the detailed description of vegetation that includes fuel moisture, the interaction with other fuels encapsulated in our method as the boundary fuel model, and a validation over a number of key wildfire phenomena such as different wildfire types and wildfire anatomical parts. To accomplish this, we propose a method that is composed of several spatial domains where heat transfer and combustion occur with some parts of the model relying on higher-scale abstractions in the form of steady-state solutions, e.g. ember ignition of vegetation. These choices where made based on analytical and empirical studies

Fig. 16. By modulating overall fuel moisture content in the boundary fuel layer and plant modules our wildfire model allows the simulation of different wildfire dynamics, ranging from various types of surface fires (a,b) to crown fires (c-e).

Table 1. Overview of the different parameter value configurations of simulations presented in Fig. 16. For each scene, the spatial dimensions are x = 70, y = 48, z = 128 with a spatial resolution (Δx) of 1 meter, $\boldsymbol{\varpi_d} = 0.15$, $\boldsymbol{\varpi_f} = 0.1$, $\boldsymbol{\varpi_g} = 0.1$, and a constant time step size of $\Delta t = 0.0125$ s. The wind force for all scenes is set at 12 m/s. There were a total of 3749 plants in the scene composed of 114550 modules. Each simulation scene is characterized by the exact same setup except we vary the eight variables: W_{min}, $\psi_{\mathcal{M}}$, ϖ_g, ψ_g, ϖ_f, ψ_f, ϖ_d, and ψ_d.

Figure	Scene	W_{min}	$\psi_{\mathcal{M}}$	ψ_g	ψ_f	ψ_d
Fig. 16a	Wildfire Rank 2	0.4	1.0	0.36	0.48	0.36
Fig. 16b	Wildfire Rank 3	0.4	1.0	0.1	0.32	0.24
Fig. 16c	Wildfire Rank 4	0.3	1.0	0.1	0.32	0.24
Fig. 16d	Wildfire Rank 5	0.5	0.7	0.07	0.2	0.16
Fig. 16e	Wildfire Rank 6	0.5	0.5	0.05	0.16	0.12

investigating wildfires as outlined throughout the paper. While this may limit the predictive power of our model, the main motivation underlying our design principles lies in the interactive simulation of visually realistic wildfires. Such models are especially useful in the context of large-scale synthetic data generation for AI model training where real, labeled data is difficult to obtain.

The validation against a controlled burn experiment indicates that our model can accurately simulate wildfire progression under certain conditions. As indicated by our results, our method offers intuitive control for generating wildfires of variable severity and type by manually setting fuel moisture parameters or managing the vegetation distribution in the scene. Furthermore, many aspects of our model could be calibrated using empirical observations or established analytical approaches such as fire spread rates provided by the Rothermel model [Andrews 2018] to increase usefulness towards real-world applications, as discussed in Sec. 6.2.

One of the main limitations of our framework is the scale of the scenes we are currently able to process (Fig. 17). While the geometric detail of vegetation significantly improves the fidelity of wildfire simulations, it imposes considerable memory demands that limit the size of the ecosystems we can simulate in real-time. This constraint presents a challenge in the context of real-world wildfires, which often span vast geographical areas. We need to address this memory limitation in order to realize the full potential of our simulation in the accurate prediction and management of large-scale wildfires. Our simulation would also benefit from a more detailed soil model to better represent the contribution of ground fires, the inclusion of fire-induced phenomena such fire whirls, which can significantly

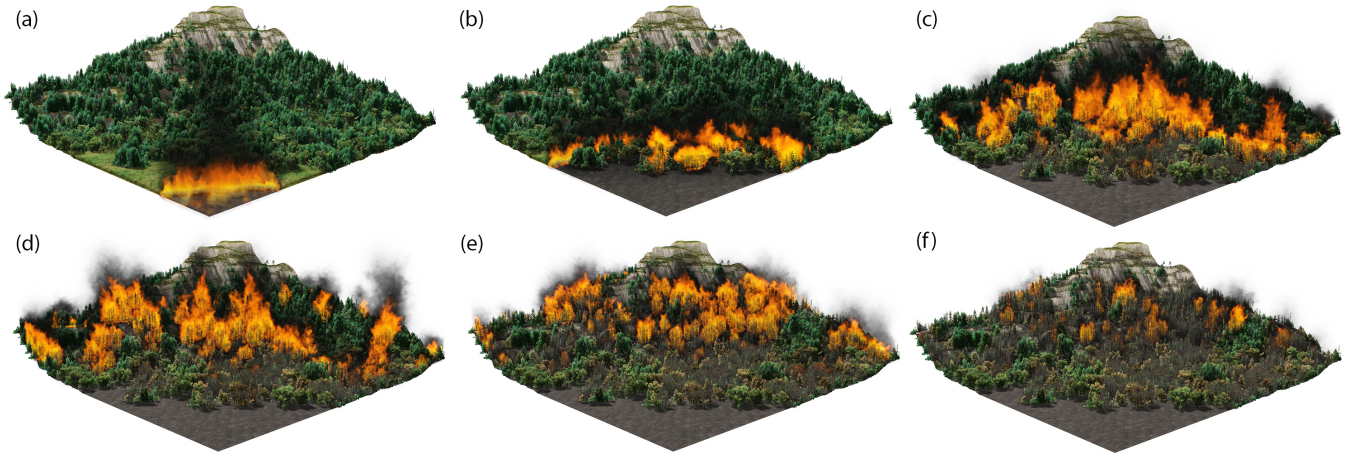

Fig. 17. A larger wildfire scene with around 200K plants composed of almost 1000K modules simulated at interactive rates. The wildfire starts as a grass fire progressing towards a forest edge (a). Once the fireline enters the forest some trees start combusting while others resist ignition due to the effects of fuel moisture (b). Eventually, the wildfire spreads to the crowns of trees and becomes more destructive (c). Due to the burning crowns a lot of firebrands are generated which cause new fire sources ahead of the fireline (d). The wildfire progresses in a complex fireline higher up the mountain side (e). Finally, as most of the fuel is consumed by the flames the wildfire wanes and exposes the burnt down trees in the forest (f).

influence fire spread and intensity. We also aim to refine our model parameters and assumptions based on further validation studies and expert feedback.

9 CONCLUSION

In this paper, we have presented a novel model for wildfire simulations that offers several significant advancements over existing models in the field. Our model captures key wildfire behaviors, such as surface, ground, and crown fires, in an accurate and computationally efficient manner. One of the major strengths of our model lies in its ability to simulate wildfires across various biomes, a feature that contributes to its broad applicability. These phenomena could not be simulated before and advance the state-of-the-art in computer graphics and beyond. Moreover, the model has been validated using real-world controlled burn experiments in fields, demonstrating its capability to reproduce important features of fireline progression. Our innovative approach to fuel moisture modeling allows us to dynamically track moisture content in fuels and to set up complex vegetation scenes for wildfire simulations. Vegetation distribution is an important factor in wildfire behavior which means that the explicit consideration of a detailed vegetation model as well as a boundary fuel layer enhances the realism of our simulation.

Unlike many existing wildfire simulations, our model operates at interactive timescales, a significant advantage that opens up possibilities for real-time or near-real-time applications, especially beneficial for firefighting services. Our model shows to be a promising tool for both research and practical applications in wildfire management. Looking forward, we see several avenues for further improvement. One key focus will be the ability to simulate larger wildfire scenes. The scale of wildfires is a significant factor in their development and visual impression, and our aim is to accurately capture these large-scale phenomena in our simulations. To achieve this, we plan to employ level-of-detail techniques, which will help manage the computational cost while maintaining the visual realism. Another area of potential development is expanding the comparisons of our model with real-world historical wildfires. Such comparisons will provide additional validations of the model's accuracy and will further enhance our understanding of wildfire dynamics and its visual representation. In conclusion, the advancements introduced in this study offer substantial potential for improving the visual realism and interactivity of wildfire simulations. We anticipate that our work will inspire further research and innovation in the field of computer graphics, particularly toward the simulation of complex natural phenomena.

ACKNOWLEDGMENTS

This work was partially supported by KAUST through the baseline funding of the Computational Sciences Group within the Visual Computing Center. The helpful discussions with Torsten Hädrich and the reviewers' valuable comments are gratefully acknowledged.

REFERENCES

N. J. Abram, B. J. Henley, A. Sen Gupta, T. J. R. Lippmann, H. Clarke, A. J. Dowdy, J. J. Sharples, R. H. Nolan, T. Zhang, M. J. Wooster, J. B. Wurtzel, K. J. Meissner, A. J. Pitman, A. M. Ukkola, B. P. Murphy, N. J. Tapper, and M. M. Boer. 2021. Connections of climate change and variability to large and extreme forest fires in southeast Australia. *Communications Earth & Environment* 2, 1 (07 Jan 2021), 8.

S. Adusumilli, J. E. Chaplen, and D. L. Blunck. 2021. Firebrand Generation Rates at the Source for Trees and a Shrub. *Frontiers in Mechanical Engineering* 7 (2021).

C. Anand, B. Shotorban, S. Mahalingam, S. McAllister, and D. Weise. 2017. Physics-Based Modeling of Live Wildland Fuel Ignition Experiments in the FIST Apparatus. *Combustion Science and Technology* 189 (03 2017).

P. L. Andrews. 2018. *The Rothermel surface fire spread model and associated developments: A comprehensive explanation.* Technical Report.

M. Aono and T. Kunii. 1984. Botanical Tree Image Generation. *IEEE Comput. Graph. Appl.* 4(5) (1984), 10–34.

E. Aragoneses and E. Chuvieco. 2021. Generation and Mapping of Fuel Types for Fire Risk Assessment. *Fire* 4, 3 (2021).

O. Argudo, C. Andújar, A. Chica, E. Guérin, J. Digne, A. Peytavie, and E. Galin. 2017. Coherent multi-layer landscape synthesis. *The Visual Computer* 33, 6 (2017), 1005–1015.

O. Argudo, E. Galin, A. Peytavie, A. Paris, and E. Guérin. 2020. Simulation, Modeling and Authoring of Glaciers. *ACM Trans. Graph. (SIGGRAPH Asia 2020)* 39, 6 (2020).

V. Babrauskas. 2003. Ignition handbook: principles and applications to fire safety engineering, fire investigation, risk management and forensic science. *Issaquah,*

WA, Fire Science Publishers 9 (2003).
S. Behrendt, C. Colditz, O. Franzke, J. Kopf, and O. Deussen. 2005. Realistic real-time rendering of landscapes using billboard clouds. *CGF* 24, 3 (2005), 507–516.
B. Benes, N. Andrysco, and O. Šťava. 2009. Interactive Modeling of Virtual Ecosystems. In *Proceedings of the Fifth Eurographics Conference on Natural Phenomena (NPH'09)*. Eurographics Association, Goslar, DEU, 9–16.
J. Bishop. 2007. Technical background of the fireline assessment method (FLAME). In *The Fire Environment–Innovations, Management, and Policy Conference Proceedings*. 27–74.
C. F. Bohren and D. B. Thorud. 1973. Two theoretical models of radiation heat transfer between forest trees and snowpacks. *Agric. For. Meteorol.* 11 (1973), 3 – 16.
D. Bradley, D. Nowrouzezahrai, and P. Beardsley. 2013. Image-based Reconstruction Synthesis of Dense Foliage. *ACM Trans. Graph.* 32, 4, Article 74 (2013), 74:1–74:10 pages.
R. Bridson and M. Müller. 2007. Fluid simulation: SIGGRAPH course notes. (2007), 1–81.
E. Bruneton and F. Neyret. 2012. Real–time Realistic Rendering and Lighting of Forests. *Comput. Graph. Forum* 31, 2pt1 (2012), 373–382.
N. P. Cheney, J. S. Gould, and W. R. Catchpole. 1993. The Influence of Fuel, Weather and Fire Shape Variables on Fire-Spread in Grasslands. *International Journal of Wildland Fire* 3, 1 (1993), 31–44.
N. Chiba, K. Muraoka, H. Takahashi, and M. Miura. 1994. Two-dimensional visual simulation of flames, smoke and the spread of fire. *JVCA* 5, 1 (1994), 37–53.
M. Cieslak, U. Govindarajan, A. Garcia, A. Chandrashekar, T. Hädrich, A. Mendoza-Drosik, D. L. Michels, S. Pirk, C.-C. Fu, and W. Palubicki. 2024. Generating Diverse Agricultural Data for Vision-Based Farming Applications. *IEEE Conference on Computer Vision and Pattern Recognition (CVPR) Workshop: Vision for Agriculture* (2024).
J. L. Coen. 2013. Modeling wildland fires : A description of the Coupled Atmosphere-Wildland Fire Environment model (CAWFE).
G. Cordonnier, P. Ecormier, E. Galin, J. Gain, B. Benes, and M.-P. Cani. 2018. Interactive Generation of Time-evolving, Snow-Covered Landscapes with Avalanches. *CGF* 37, 2 (2018), 497–509.
G. Cordonnier, E. Galin, J. Gain, B. Benes, E. Guérin, A. Peytavie, and M.-P. Cani. 2017. Authoring Landscapes by Combining Ecosystem and Terrain Erosion Simulation. *ACM Trans. Graph.* 36, 4, Article 134 (2017), 12 pages.
O. Deussen, P. Hanrahan, B. Lintermann, R. Měch, M. Pharr, and P. Prusinkiewicz. 1998. Realistic Modeling and Rendering of Plant Ecosystems. *ACM Trans. Graph.* (1998), 275–286.
J.-L. Dupuy and M. Larini. 2000. Fire spread through a porous forest fuel bed: a radiative and convective model including fire-induced flow effects. *International Journal of Wildland Fire* 9, 3 (2000), 155–172.
L. H. Encinas, S. H. White, A. M. del Rey, and G. R. Sánchez. 2007. Modelling forest fire spread using hexagonal cellular automata. *Appl. Math. Model.* 31, 6 (2007), 1213 – 1227.
R. Fedkiw, J. Stam, and H. W. Jensen. 2001. Visual Simulation of Smoke. *Proc. of ACM SIGGRAPH* (2001), 15–22.
J.-B. Filippi, F. Bosseur, C. Mari, and C. Lac. 2018. Simulation of a Large Wildfire in a Coupled Fire-Atmosphere Model. *Atmosphere* 9 (06 2018), 218.
A. Galgano and C. Di Blasi. 2005. Infinite- versus finite-rate kinetics in simplified models of wood pyrolysis. *Combustion Science and Technology* 177 (2005), 279–303.
C. Godin and Y. Caraglio. 1998. A Multiscale Model of Plant Topological Structures. *Journal of Theoretical Biology* 191, 1 (1998), 1–46.
U. I. Gol'dshleger, K. V. Pribytkova, and V. V. Barzykin. 1973. Ignition of a condensed explosive by a hot object of finite dimensions. *Combustion, Explosion and Shock Waves* 9 (1973), 99–102.
J. Guo, H. Jiang, B. Benes, O. Deussen, X. Zhang, D. Lischinski, and H. Huang. 2020. Inverse Procedural Modeling of Branching Structures by Inferring L-Systems. 39, 5, Article 155 (June 2020), 13 pages.
R. Habel, A. Kusternig, and M. Wimmer. 2009. Physically Guided Animation of Trees. *Comp. Graph. Forum* 28, 2 (2009), 523–532.
R. M. Hadden, S. Scott, C. Lautenberger, and A. C. Fernandez-Pello. 2011. Ignition of Combustible Fuel Beds by Hot Particles: An Experimental and Theoretical Study. *Fire Technology* 47 (2011), 341–355.
T. Hädrich, D. T. Banuti, W. Pałubicki, S. Pirk, and D. L. Michels. 2021. Fire in Paradise: Mesoscale Simulation of Wildfires. *ACM Trans. on Graph.* 40, 4, Article 163 (2021).
T. Hädrich, B. Benes, O. Deussen, and S. Pirk. 2017. Interactive Modeling and Authoring of Climbing Plants. *CGF* 36, 2 (2017), 49–61.
T. Hädrich, M. Makowski, W. Pałubicki, D. T. Banuti, S. Pirk, and D. L. Michels. 2020. Stormscapes: Simulating Cloud Dynamics in the Now. *ACM Trans. Graph.* 39, 6, Article 175 (Nov. 2020), 16 pages.
J. A. A. Herrera, T. Hädrich, W. Pałubicki, D. T. Banuti, S. Pirk, and D. L. Michels. 2021. Weatherscapes: Nowcasting Heat Transfer and Water Continuity. *ACM Transaction on Graphics* 40, 6, Article 204 (12 2021).
Y. Hong, D. Zhu, X. Qiu, and Z. Wang. 2010. Geometry-based Control of Fire Simulation. *Vis. Comput.* 26, 9 (2010), 1217–1228.
C. Horvath and W. Geiger. 2009. Directable, High-Resolution Simulation of Fire on the GPU. *ACM Trans. Graph.* 28, 3, Article 41 (July 2009), 8 pages.
Z. Huang, G. Gong, and L. Han. 2014. Physically-based modeling, simulation and rendering of fire for computer animation. *Multimedia Tools and Applications* 71, 3 (01 Aug 2014), 1283–1309.
T. Ijiri, S. Owada, and T. Igarashi. 2006. Seamless Integration of Initial Sketching and Subsequent Detail Editing in Flower Modeling. *Comp. Graph. Forum* 25, 3 (2006), 617–624.
R. J. Innes. 2013. Fire regimes of Alaskan tundra communities. www.fs.usda.gov/database/feis/fire_regimes/AK_tundra/all.html. Accessed: 2024-04-16.
M. Jaeger and J. Teng. 2003. Tree and plant volume imaging - An introductive study towards voxelized functional landscapes. *PMA* (2003).
J. Jones. 1993. Predictive Calculations of the Effect of an Accidental Heat Source on a Bed of Forest Litter. *Journal of Fire Sciences* 11, 1 (1993), 80–86.
J. Jones. 1994. Further Calculations Regarding the Accidental Supply of Heat to a Bed of Forest Material. *Journal of Fire Sciences* 12, 6 (1994), 502–505.
J. Kałużny, Y. Schreckenberg, K. Cyganik, P. Annighöfer, S. Pirk, D. Michels, M. Cieslak, F. Assaad, B. Benes, and W. Palubicki. 2024. LAESI: Leaf Area Estimation with Synthetic Imagery. *IEEE Conference on Computer Vision and Pattern Recognition (CVPR) Workshop: Synthetic Data for Computer Vision* (2024).
K. Kapp, J. Gain, E. Guérin, E. Galin, and A. Peytavie. 2020. Data-driven Authoring of Large-scale Ecosystems. *ACM Trans. Graph.* (2020).
J. Katan and L. Perez. 2021. ABWiSE v1.0: toward an agent-based approach to simulating wildfire spread. *Natural Hazards and Earth System Sciences* 21, 10 (2021), 3141–3160.
A. Lamorlette and N. Foster. 2002. Structural Modeling of Flames for a Production Environment. In *Proceedings of the 29th Annual Conference on Computer Graphics and Interactive Techniques (SIGGRAPH '02)*. ACM, New York, NY, USA, 729–735.
B. Lane and P. Prusinkiewicz. 2002. Generating Spatial Distributions for Multilevel Models of Plant Communities. *Graphics Interface* (2002), 69–80.
M. J. Lawes, A. Richards, J. Dathe, and J. J. Midgley. 2011. Bark thickness determines fire resistance of selected tree species from fire-prone tropical savanna in north Australia. *Plant Ecol.* 212, 12 (2011), 2057–2069.
B. Li, J. Kałużny, J. Klein, D. L. Michels, W. Pałubicki, B. Benes, and S. Pirk. 2021. Learning to Reconstruct Botanical Trees from Single Images. *ACM Trans. Graph.* 40, 6, Article 231 (12 2021).
B. Li, J. Klein, D. L. Michels, B. Benes, S. Pirk, and W. Palubicki. 2023. Rhizomorph: The Coordinated Function of Shoots and Roots. *ACM Trans. Graph.* 42, 4 (8 2023).
B. Lintermann and O. Deussen. 1999. Interactive Modeling of Plants. *IEEE Comput. Graph. Appl.* 19, 1 (Jan. 1999), 56–65.
S. Liu, T. An, Z. Gong, and I. Hagiwara. 2012. *Physically Based Simulation of Solid Objects Burning.* Springer Berlin Heidelberg, Berlin, Heidelberg, 110–120.
Y. Liu, J. Guo, B. Benes, O. Deussen, X. Zhang, and H. Huang. 2021. TreePartNet: Neural Decomposition of Point Clouds for 3D Tree Reconstruction. *ACM Trans. Graph.* 40, 6, Article 232 (dec 2021), 16 pages.
Y. Livny, S. Pirk, Z. Cheng, F. Yan, O. Deussen, D. Cohen-Or, and B. Chen. 2011. Texture-lobes for Tree Modelling. *ACM Trans. Graph.* 30, 4, Article 53 (2011), 10 pages.
Y. Lizhong, C. Xiaojun, Z. Xiaodong, and F. Weicheng. 2002. A modified model of pyrolysis for charring materials in fire. *Int. J. Eng. Sci.* 40, 9 (2002), 1011 – 1021.
S. Longay, A. Runions, F. Boudon, and P. Prusinkiewicz. 2012. TreeSketch: interactive procedural modeling of trees on a tablet. In *Proc. of the Intl. Symp. on SBIM*. 107–120.
F. Maggioli, J. Klein, T. Hädrich, E. Rodolà, W. Pałubicki, S. Pirk, and D. L. Michels. 2023. A Physically-inspired Approach to the Simulation of Plant Wilting. In *SIGGRAPH Asia 2023 Conference Papers*. ACM, New York, NY, USA, Article 66, 8 pages.
M. Makowski, T. Hädrich, J. Scheffczyk, D. L. Michels, S. Pirk, and W. Pałubicki. 2019. Synthetic Silviculture: Multi-Scale Modeling of Plant Ecosystems. *ACM Trans. Graph.* 38, 4, Article 131 (2019), 14 pages.
J. Mandel, A. Kochanski, M. Vejmelka, and J. Beezley. 2014. Data Assimilation of Satellite Fire Detection in Coupled Atmosphere-Fire Simulation by WRF-SFIRE. (10 2014).
S. L. Manzello, A. Maranghides, J. R. Shields, W. E. Mell, Y. Hayashi, and D. Nii. 2009. Mass and size distribution of firebrands generated from burning Korean pine (Pinus koraiensis) trees. *Fire and Materials* 33, 1 (2009), 21–31.
M. M. Masinda, L. Sun, G. Wang, and T. Hu. 2020. Moisture content thresholds for ignition and rate of fire spread for various dead fuels in northeast forest ecosystems of China. *Journal of Forestry Research* (05 Jun 2020).
S. McAllister, J. Chen, and A. Fernandez-Pello. 2011. *Fundamentals of Combustion Processes.* Springer New York.
K. McGrattan, R. McDermott, J. Floyd, S. Hostikka, G. Forney, and H. Baum. 2012. Computational fluid dynamics modelling of fire. *International Journal of Computational Fluid Dynamics* 26, 6-8 (2012), 349–361.
Z. Melek and J. Keyser. 2002. Interactive simulation of fire. *Pacific Graphics* (2002), 431–432.
W. Mell, M. A. Jenkins, J. Gould, and P. Cheney. 2007. A physics-based approach to modelling grassland fires. *International Journal of Wildland Fire* 16, 1 (2007), 1–22.
H. Mendoza, A. Brown, and A. Ricks. 2019. Modeling High Heat Flux Combustion of Coniferous Trees Using Chemically Reacting Lagrangian Particles *(WSSCI Fall Technical Meeting of the Western States Section of the Combustion Institute).*

S. Monedero, J. Ramirez, D. Molina-Terrén, and A. Cardil. 2017. Simulating wildfires backwards in time from the final fire perimeter in point-functional fire models. *Environmental Modelling & Software* 92 (2017), 163 – 168.
R. Měch and P. Prusinkiewicz. 1996. Visual models of plants interacting with their environment. In *Proc. of SIGGRAPH*. ACM, 397–410.
B. Neubert, T. Franken, and O. Deussen. 2007. Approximate Image-based Tree-modeling Using Particle Flows. *ACM Trans. Graph.* 26, 3, Article 88 (2007).
B. Neubert, S. Pirk, O. Deussen, and C. Dachsbacher. 2011. Improved Model- and View-Dependent Pruning of Large Botanical Scenes. *Comp. Graph. Forum* 30, 6 (2011), 1708–1718.
D. Q. Nguyen, R. Fedkiw, and H. W. Jensen. 2002. Physically Based Modeling and Animation of Fire. *ACM Trans. Graph.* 21, 3 (2002), 721–728.
D. Q. Nguyen, R. P. Fedkiw, and M. Kang. 2001. A Boundary Condition Capturing Method for Incompressible Flame Discontinuities. *J. Comput. Phys.* 172, 1 (2001), 71 – 98.
M. B. Nielsen, M. Bojsen-Hansen, K. Stamatelos, and R. Bridson. 2022. Physics-Based Combustion Simulation. *ACM Trans. Graph.* 41, 5, Article 176 (may 2022), 21 pages.
T. Niese, S. Pirk, M. Albrecht, B. Benes, and O. Deussen. 2022. Procedural Urban Forestry. *ACM Transaction on Graphics* 41, 1 (2022).
M. Okabe, S. Owada, and T. Igarashi. 2007. Interactive Design of Botanical Trees Using Freehand Sketches and Example-based Editing. In *ACM SIGGRAPH Courses*. ACM, Article 26.
P. E. Oppenheimer. 1986. Real time design and animation of fractal plants and trees. *Proc. of SIGGRAPH* 20, 4 (1986), 55–64.
W. Palubicki, K. Horel, S. Longay, A. Runions, B. Lane, R. Měch, and P. Prusinkiewicz. 2009. Self-organizing Tree Models for Image Synthesis. 28, 3, Article 58 (2009), 58:1–58:10 pages.
W. Pałubicki, M. Makowski, W. Gajda, T. Hädrich, D. L. Michels, and S. Pirk. 2022. Ecoclimates: Climate-response Modeling of Vegetation. *ACM Trans. Graph.* 41, 4, Article 155 (July 2022), 19 pages.
Z. Pan and D. Manocha. 2017. Efficient Solver for Spacetime Control of Smoke. *ACM Trans. Graph.* 36, 5, Article 162 (July 2017), 13 pages.
A. Paris, E. Galin, A. Peytavie, E. Guérin, and O. Argudo. 2019. Desertscapes Simulation. *CGF* 38, 7 (2019).
E. Pastor, L. Zárate, E. Planas, and J. Arnaldos. 2003. Mathematical models and calculation systems for the study of wildland fire behaviour. *Progress in Energy and Combustion Science* 29, 2 (2003), 139 – 153.
W. Pałubicki, A. Kokosza, and A. Burian. 2019. Formal description of plant morphogenesis. *Journal of Experimental Botany* 70, 14 (07 2019), 3601–3613.
V. Pegoraro and S. G. Parker. 2006. Physically-Based Realistic Fire Rendering. In *Eurographics Workshop on Natural Phenomena*. The Eurographics Association.
A. Peytavie, T. Dupont, E. Guérin, Y. Cortial, B. Benes, J. Gain, and E. Galin. 2019. Procedural Riverscapes. *CGF* 38, 7 (2019), 35–46.
M. Pharr, W. Jakob, and G. Humphreys. 2016. *Physically Based Rendering: From Theory to Implementation* (3rd ed.). Morgan Kaufmann Publishers Inc., San Francisco, USA.
S. Pirk, M. Jarząbek, T. Hädrich, D. L. Michels, and W. Palubicki. 2017. Interactive Wood Combustion for Botanical Tree Models. *ACM Trans. Graph.* 36, 6, Article 197 (2017).
S. Pirk, T. Niese, O. Deussen, and B. Neubert. 2012a. Capturing and Animating the Morphogenesis of Polygonal Tree Models. *ACM Trans. Graph.* 31, 6, Article 169 (2012), 169:1–169:10 pages.
S. Pirk, T. Niese, T. Hädrich, B. Benes, and O. Deussen. 2014. Windy Trees: Computing Stress Response for Developmental Tree Models. *ACM Trans. Graph.* 33, 6, Article 204 (2014), 11 pages.
S. Pirk, O. Stava, J. Kratt, M. A. M. Said, B. Neubert, R. Měch, B. Benes, and O. Deussen. 2012b. Plastic trees: interactive self-adapting botanical tree models. *ACM Trans. Graph.* 31, 4, Article 50 (2012), 10 pages.
P. Prusinkiewicz. 1986. Graphical applications of L-systems. In *Proc. on Graph. Interf.* 247–253.
L. Quan, P. Tan, G. Zeng, L. Yuan, J. Wang, and S. B. Kang. 2006. Image-Based Plant Modeling. *ACM Trans. Graph.* 25, 3 (2006), 599–604.
E. Quigley, Y. Yu, J. Huang, W. Lin, and R. Fedkiw. 2018. Real-Time Interactive Tree Animation. 24, 5 (2018), 1717–1727.
N. Rasmussen, D. Q. Nguyen, W. Geiger, and R. Fedkiw. 2003. Smoke Simulation for Large Scale Phenomena. *ACM Trans. Graph.* 22, 3 (July 2003), 703–707.
G. D. Richards. 1990. An elliptical growth model of forest fire fronts and its numerical solution. *Internat. J. Numer. Methods Engrg.* 30, 6 (1990), 1163–1179.
A. Runions, B. Lane, and P. Prusinkiewicz. 2007. Modeling Trees with a Space Colonization Algorithm. *EG Nat. Phenom.* (2007), 63–70.
L. Schiller and Z. Naumann. 1935. A Drag Coefficient Correlation. *VDI Zeitung* 77 (1935), 318–320.
D. W. Schwilk. 2003. Flammability Is a Niche Construction Trait: Canopy Architecture Affects Fire Intensity. *The American Naturalist* 162, 6 (2003), 725–733.
A. Selle, R. Fedkiw, B. Kim, Y. Liu, and J. Rossignac. 2008. An unconditionally stable MacCormack method. *Journal of Scientific Computing* 35 (2008), 350–371.
H. Shao, T. Kugelstadt, T. Hädrich, W. Pałubicki, J. Bender, S. Pirk, and D. L. Michels. 2021. Accurately Solving Rod Dynamics with Graph Learning. In *NeurIPS*.
J. Stam. 1999. Stable Fluids. In *Proceedings of the 26th Annual Conference on Computer Graphics and Interactive Techniques (SIGGRAPH '99)*. ACM Press/Addison-Wesley Publishing Co., USA, 121–128.
O. Stava, S. Pirk, J. Kratt, B. Chen, R. Měch, O. Deussen, and B. Benes. 2014. Inverse Procedural Modelling of Trees. *Computer Graphics Forum* (2014), n/a–n/a.
A. Stomakhin, C. Schroeder, C. Jiang, L. Chai, J. Teran, and A. Selle. 2014. Augmented MPM for Phase-change and Varied Materials. *ACM Trans. Graph.* 33, 4, Article 138 (2014), 11 pages.
P. Tan, T. Fang, J. Xiao, P. Zhao, and L. Quan. 2008. Single Image Tree Modeling. *ACM Trans. Graph.* 27, 5, Article 108 (2008), 7 pages.
A. Tohidi, N. Kaye, and W. Bridges. 2015. Statistical description of firebrand size and shape distribution from coniferous trees for use in Metropolis Monte Carlo simulations of firebrand flight distance. *Fire Safety Journal* 77 (2015), 21–35.
M. Vanella, K. McGrattan, R. McDermott, G. Forney, W. Mell, E. Gissi, and P. Fiorucci. 2021. A Multi-Fidelity Framework for Wildland Fire Behavior Simulations over Complex Terrain. *Atmosphere* 12, 2 (2021).
U. Vimont, J. Gain, M. Lastic, G. Cordonnier, B. Abiodun, and M.-P. Cani. 2020. Interactive Meso-scale Simulation of Skyscapes. *CGF* 39, 2 (2020), 585–596.
S. Whitaker. 1972. Forced convection heat transfer correlations for flow in pipes, past flat plates, single cylinders, single spheres, and for flow in packed beds and tube bundles. *AIChE Journal* 18, 2 (1972), 361–371.
J. Wither, F. Boudon, M.-P. Cani, and C. Godin. 2009. Structure from silhouettes: a new paradigm for fast sketch-based design of trees. 28, 2 (2009), 541–550.
S.-K. Wong and K.-C. Chen. 2015. A Procedural Approach to Modelling Virtual Climbing Plants With Tendrils. *Comput. Graph. Forum* (2015).
H. Xu, N. Gossett, and B. Chen. 2007. Knowledge and heuristic-based modeling of laser-scanned trees. 26, 4 (2007), Article 19, 13 pages.
Y. Zhao, X. Wei, Z. Fan, A. Kaufman, and H. Qin. 2003. Voxels on fire [computer animation]. In *IEEE Visualization, 2003. VIS 2003.* 271–278.
X. Zhou, B. Li, B. Benes, S. Fei, and S. Pirk. 2023. DeepTree: Modeling Trees with Situated Latents. *IEEE TVCG* (2023), 1–14.
P. Zylstra. 2021. Linking fire behaviour and its ecological effects to plant traits, using FRaME in R. *Methods in Ecology and Evolution* 12, 8 (2021), 1365–1378.

A APPENDIX

A.1 Vegetation Model

We compute the environmental adaptation parameter $o \in [0, 1]$ of a given plant based on local temperature and soil water availability as proposed by [Makowski et al. 2019]. We sample the soil water availability q_w and atmospheric temperature T_a at the position where the plant is located. Next we compute a climatic adaptation parameter o as follows:

$$o = \frac{\mathcal{N}_T(T_a) \cdot \mathcal{N}_P(q_w)}{\mathcal{N}_T(T_A) \cdot \mathcal{N}_P(P_A)}, \tag{26}$$

where $\mathcal{N}_T(\cdot)$ and $\mathcal{N}_P(\cdot)$ denote the normal distributions of temperature and soil water, and T_A and P_A are plant type parameters defining the climatic adaptation of plant species to temperature and humidity.

Next, we evaluate light exposure values of the atmosphere space and propagate them as light flux through the plant graph H. Specifically, we sample the light exposure at the locations of all end nodes of plant graph H (except root nodes) and set light flux values Q_i of modules equal to light exposure values L. Then we propagate the values of light exposure as light flux Q of all end nodes downwards through the graph H summing them together at each module bifurcation point:

$$Q_i = Q_m + Q_c, \tag{27}$$

where Q_m denotes light flux from the main module and Q_c the light flux of the child module until the total light exposure value of all end nodes is computed at the base node as total light flux Q_p.

After calculating the light flux, we calculate the vigor values from the base node to the end nodes of the plant graph H. The vigor of a module is a measure of its physiological activity and health, which

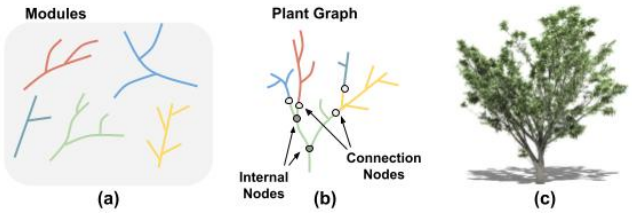

Fig. 18. Our plant representation is module-based: Each plant is defined as a combination of modules (a), which are reused across the ecosystem by exploiting the repetitive structure of plants (b). After defining the branch graph, we generate the final plant geometry from the module-based graph description (c).

directly impacts its moisture content. Starting with the base node we determine the total vigor V_{root} available for the plant as

$$V_{root} = Q_p \cdot o\,. \tag{28}$$

This means that total vigor of a plant depends both on the total light availability to modules as well as its overall climatic adaptation to local temperature and soil water. Once we have computed the total vigor for the base module, we propagate vigor V as vigor flux upwards in the plant graph H by allocating vigor flux to main or child modules. At each branching point, we determine the distribution of vigor towards the next node of the current module (V_m) and the node of the child module (V_c) based on the vigor of the parent module (V_p):

$$V_m = V_p \cdot \frac{\lambda(Q_m)}{\lambda(Q_m) + (1-\lambda)(Q_c)}\,, \tag{29}$$

$$V_c = (V_p - V_m)\,. \tag{30}$$

where the weight λ corresponds to the one introduced in [Palubicki et al. 2009], which is used to distinguish species-dependent preferences to develop vigorous branches. The notion of vigor in our model therefore conceptualizes the impact of local light conditions as well as species-dependent traits.

A.2 Frank-Kamenetskii hot spot parameter

We estimate the dimensionless Frank-Kamenetskii hot spot parameter δ_{cr} at which thermal runaway (ignition) occurs as:

$$b = \frac{\rho_g C p_g}{\rho_e C p_e}\,, \quad \beta = \frac{RT_e}{E}\,, \quad \theta_0 = \frac{E}{RT_e^2}\left(T_e - T_g\right)\,, \tag{31}$$

$$\delta_{cr} \approx 0.4\sqrt{b^2 + 1.5\left(b + 0.1b^3\right)}\,(2.25 - \theta_0)^2\,(1 - 0.5\beta\theta_0)\,, \tag{32}$$

where Cp_g, ρ_g, E, T_g, and R are the specific heat of the grass, grass density, grass activation energy, grass temperature, and ideal gas constant.

A.3 Scene Setup Parameters

L	Light exposure values
T_A, L_A, P_A	Adaptive parameters response to temperature, light, and soil water, respectively, for a given plant species or grass
$\varpi_g, \varpi_f, \varpi_d$	Maximum biomass of grass, fine fuel, and duff, respectively
$\mathcal{M}$	A module in a plant structure
$G_{\mathcal{M}}$	A graph describing a module
M	Mass of a plant module
Q	Light Flux of a plant module
v	Vigor of a plant module
$\mathcal{P}$	A plant
$H_{\mathcal{P}}$	A graph describing a plant
φ_f	Average fine fuel production of a plant
σ_f	Fine fuel spread of a plant
κ_p	Transpiration rate
o	Environmental adaptation parameter of a plant
Q_p	Total light flux available to the plant
V_{root}	Total vigor available to the plant
λ	Species-dependent preference to develop vigorous branches at the apex
ψ	Moisture content per plant species
W_{min}	Minimum fuel moisture value for a given plant species
B_g, B_f, B_d	Biomass value of a grid cell for grass, fine fuel, and duff layers, respectively
$G_f(x, y)$	Fine fuel kernel function
$G_d(x, y)$	Duff kernel function
σ_f	Standard deviation of the Gaussian in fine fuel kernel
μ_d^{opt}	Optimal moisture value for decomposition

A.4 Wildfire Simulation Parameters

T_a	Atmospheric temperature (°C)
q_v	Vapor content in the atmospheric model (kg/m^3)
q_s	Smoke in the atmosphere grid cell
u	Wind speed (m/s)
T_g, T_f, T_d	Temperature of grass, fine fuel, and duff, respectively (°C)
W_g, W_f, W_d	Moisture content of grass, fine fuel, and duff (%)
W	Moisture of a plant module (%)
Δq_w	Water diffusion in the soil ($kg/m^3 \cdot m/s$)
k	Reaction rate of the combusting fuel (rate units)
$T_{\mathcal{M}}$	Temperature of the module (°C)
$W_{\mathcal{M}}$	Total moisture of module (%)
c	Dimensionless char insulation parameter
A	Pyrolyzing front area (m^2)
T_0, T_1	Lower and upper temperature limits for combustion (°C)
W_0, W_1	Lower and upper moisture limits for combustion (%)
η	Function describing the impact of wind on the reaction rate
u_{ref}	Optimal wind speed for maximum boost to the reaction rate (m/s)
$\boldsymbol{u}$	Velocity field (m/s)
K_{ij}	Thermal conductivity between domains i and j ($W/(m \cdot K)$)
α	Diffusion intensity
γ	Radiative cooling term
T_{amb}	Ambient temperature (°C)
M_s	Mass for grid cell (kg)
W_s	Water content in each grid cell (%)
T_m	Module's surface temperature (°C)
α_m	Diffusion coefficient for modules (m^2/s)
b	Temperature coefficient for modules
D_g, D_f, D_d	Diffusion coefficients for grass, fine fuel, and duff (m^2/s)
$\kappa_w^m(T_{\mathcal{M}})A$	Evaporation function for another module (e.g., vegetation), dependent on the module temperature $T_{\mathcal{M}}$ ($1/s$), multiplied by area A (m^2)
$S_{T_0^d, T_1^d}(T_d)$	Smoothstep function for evaporation in the duff layer, defined between two temperature limits T_0^d and T_1^d (C)
ΔH_x	combustion heat rate for specific domain x
A_g	Grass pre-exponential factor
ρ_g	Grass density (derived from biomass)
r_{cr}	Minimum particle radius necessary for ignition
E	Activation energy
R	Universal gas constant

Table 2. Performance characteristics for various wildfire simulations. The table presents the grid size, the number of trees and modules in the simulation, the memory used, and the duration of each simulation step for different scenes. The time-step is 45 seconds.

Figure	Scene	Grid Size	Cell Size	Modules	Plants	Memory	Step Duration
Fig. 17	Mountain Forest	405x405x250	1m	886,293	202,301	23GB	201.3ms
Fig. 11b	Cultivated Forest	576x320x560	0.125m	29,158	1,582	22GB	220ms
Fig. 12b	Rainforest	405x405x150	1m	254,843	61,820	12GB	65ms

A.5 Runtime Performance

A.6 MacCormack Advection

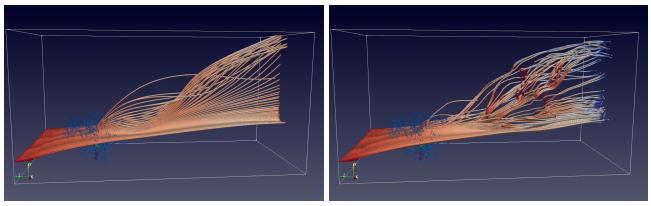

Fig. 19. A side-by-side comparison of the wildfire simulations before (left) and after (right) the application of the numerical changes in our study. The simulation domain is marked by a box with white borders, and the resolution of this domain is set at $64 \times 64 \times 128$. Visualization of both the tree and the streamlines has been accomplished using the ParaView software. Color-coding of streamlines indicates wind speeds, while tree branches are colored according to their respective radii.

A.7 Parameter Values

Table 3. Overview of the wildfire simulation parameters and their corresponding values for the ember simulation shown in Fig. 14 (g-i).

Parameter	Symbol	Value
Vorticity Confinement	c	30.0
Eta	η	10
DX	Δx	1
Initial Water Multiplier	W_{min}	0.33
Wind Velocity	$u(x, z)$	(12, 10)
Fine Fuel Burn Rate	k	1
Duff Burn Rate	ϖ_d	1
Grass Burn Rate	ϖ_g	3.7
Grass Diffusion Rate	D_g	0.8
Fine Fuel Rate	ϖ_f	0.5
Fire Temperature Cooling	γ	0.0015
Min Water Burn	W_{min}	0.03
Grass Mass	B_g	0.2
Grass Water	W_g	0.1
Fuel Mass	B_f	0.2
Fuel Water	W_f	0.8
Duff Mass	B_d	0.1
Duff Water	W_d	0.2

A.8 Ember Ablation

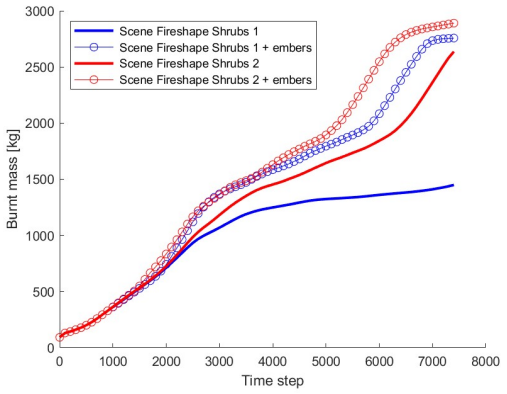

Fig. 20. This plot depicts a quantitative ablation study of the ember model shown in the results in Fig. 14. The hill-shaped blue line indicates biomass loss as a function of time for the model without embers is contrasted with a more complex curve shape of the experiment with ember model - due to the non-linear nature of wildfires with embers. The red line indicates the mass loss evolution for a drier scene. Here, the difference between the models is less noticeable.

A.9 Controlled Burn Experiments

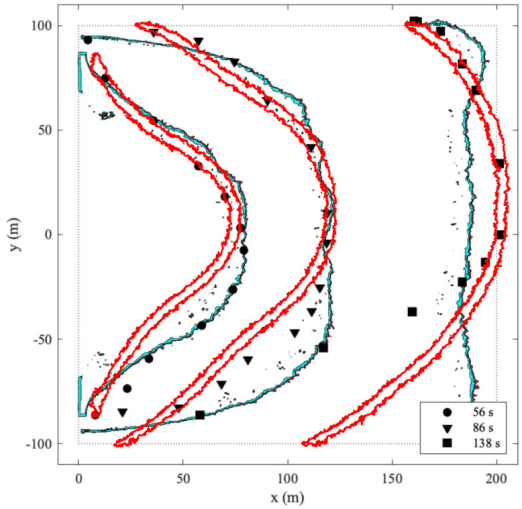

Fig. 21. We compare shapes of the fireline of a real burn experiment (dots, squares, triangles) at three different time points with our simulated fireline contour (red) and the results of a wildfire simulation conducted by Vanella et al. [2021] (teal contour). Our simulated fireline shape conforms closely in shape and progression to the real fireline of the burn experiment.